Uppsala University

Master of Science Degree in physics

Department of Physics and Astronomy
Division of Materials Theory

June 28, 2019

Best practice of extracting magnetocaloric properties in magnetic simulations

Author:
Johan Bylin

Supervisor:
Anders Bergman

UPPSALA
UNIVERSITET

Abstract

In this thesis, a numerical study of simulating and computing the magnetocaloric properties of magnetic materials is presented. The main objective was to deduce the optimal procedure to obtain the isothermal change in entropy of magnetic systems, by evaluating two different formulas of entropy extraction, one relying on the magnetization of the material and the other on the magnet's heat capacity. The magnetic systems were simulated using two different Monte Carlo algorithms, the Metropolis and Wang-Landau procedures.

The two entropy methods proved to be comparably similar to one another. Both approaches produced reliable and consistent results, though finite size effects could occur if the simulated system became too small. Erroneous fluctuations that invalidated the results did not seem stem from discrepancies between the entropy methods but mainly from the computation of the heat capacity itself. Accurate determination of the heat capacity via an internal energy derivative generated excellent results, while a heat capacity obtained from a variance formula of the internal energy rendered the extracted entropy unusable. The results acquired from the Metropolis algorithm were consistent, accurate and dependable, while all of those produced via the Wang-Landau method exhibited intrinsic fluctuations of varying severity. The Wang-Landau method also proved to be computationally ineffective compared to the Metropolis algorithm, rendering the method not suitable for magnetic simulations of this type.

Populärvetenskaplig sammanfattning

Magnetiska material har fascinerat människan sen urminnes tider, och genom aktiv forskning har magnetismens mångsidiga egenskaper kunnat tas tillvara på och tillgodogöras för teknologiskt bruk. För att förstå sig på hur magnetism kan uppstå måste man djupdyka in i atomernas värld och studera deras egenskaper och hur de interagerar med varandra. Det visar sig att elektronerna, de negativt laddade partiklarna i material, uppvisar ett magnetiskt beteende som påminner om stavmagneter; varje elektron har en magnetisk nord- och sydände. När elektronernas magnetiska riktning i ett material pekar åt samma håll adderas effekten som leder till en storskalig stark magnet, exempelvis en kylskåpsmagnet. Denna typ av magnetism kallas ferromagnetism. Pekar varje elektrons magnetiska riktning åt parvis motsatta håll så neutraliseras den storskaliga magnetismen, och på grund av det drastiskt motsatta beteendet kallas denna typ av material antiferromagnetisk. Om det är så att alla elektroners magnetiska riktning är slumpmässigt orienterade så bildas det inte heller någon storskalig magnetism, men lägger man på ett externt magnetfält så rätar elektronerna upp sig jäms med magnetfältet så att materialet faktiskt blir magnetiskt, och denna typ av magnetism kallas paramagnetism.

Vid låga temperaturer så är magneters magnetism stabil, vare sig det rör sig om ferro- eller antiferromagneter, men ökar man temperaturen så börjar varje elektrons magnetiska riktning att sakta men säkert fluktuera. Vid en viss materialspecifik temperatur, kallad den kritiska temperaturen, så är fluktuationerna så pass kraftiga att materialet plötsligt totalt tappar sin magnetism och övergår till att vara en paramagnet. Detta fenomen där materialets egenskaper drastiskt ändras från ett beteende till ett annat kallas för fasövergång, och en vardaglig analogi kan jämföras med när is smälter eller vatten kokas. Det intressanta med magnetiska fasövergångar är att de kan exploateras på ett finurligt sätt. Eftersom ett externt magnetfält kan räta tillbaka elektronernas magnetiska orientering och därmed göra materialet, till viss del, ferromagnetisk igen, så kan ett varierande externt magnetfält tvinga materialet att pendla mellan ett ferromagnetiskt och paramagnetiskt tillstånd. Detta innebär att materialet manas att genomgå flera magnetiska fasövergångar, styrt enbart av det växlande magnetfältet. Utförs denna process på rätt sätt, det vill säga att den överflödiga värmeenergin kan effektivt skingras och ledas bort från materialet, så uppstår en effektiv kylningseffekt som sänker temperaturen av ämnet. Denna företeelse kallas för magnetokalorieffekten, och en av framtidsförhoppningarna är att effekten en dag ska kunna användas i exempelvis konventionella kylskåp. Men innan dess bör lämpliga materialkandidater utses, och ett av de lämpligaste måtten som används för att avgöra magnetens prestanda är entropin, en abstrakt kvantitet som, på ett sätt, förmedlar materialets inneboende ordning och energistruktur.

I detta projekt studeras två olika sätt att ta reda på entropiförändringen hos magnetiska material som uppvisar kraftiga magnetokalorieffekter. Den ena metoden beräknar entropin via en formel som utgår från materialets storskaliga genomsnittliga magnetisering, medan den andra metoden tar reda på entropin via materialets värmekapacitet, som är ett mått på hur väl ämnet kan absorbera värmeenergi. För att testa dessa två metoder så användes ett numera vanligt förekommande arbetssätt att studera fysik, vilket då motsvarar datasimulationer. Genom att modelera och kvantisera de mångtaliga magnetiska interaktionerna som sker i en magnet så kan det simulerade materialet efterlikna en verklighetsbaserad magnet, vilket gör det möjligt att utföra sofistikerade experiment utan laboratorieutrustning. De magnetiska material som simulerades i detta projekt var först ett sorts kubiskt referensmaterial vars atomära magnetiska interaktioner bara avgränsades till sina närmaste grannar, det vill säga att varje atom bara utbytte interaktioner med sina närmaste kringliggande atomgrannar, medan atomer utanför denna krets bortsågs. Ett annat material som studerades var klassiskt järn, som vid låga temperaturer uppvisar ett ferromagnetiskt beteende men runt 1044 grader kelvin övergår till att vara paramagnetiskt. Detta material är extensivt studerat, och behandlas i många vetenskapliga kretsar som en referenspunkt för att testa noggrannheten och sanningsvärdet hos nya teorier och metoder. Sista materialet som undersöktes var ett material vid namn CoMnSi, en sammansättning av kobolt, mangan och kisel, som via experiment runt rumstemperatur har uppvisat den eftertraktade magnetokalorieffekten. Dessa tre material simulerades via två olika dataalgoritmer, en standardmetod som kallas Metropolisalgoritmen samt en nyare procedur som heter Wang-Landaumetoden.

Det visade sig att båda entropimetoderna producerade utmärkta och likartade resultat, trots att de är utsprungna från två olika teoretiska bakgrunder. De enda gångerna som dessa två metoder inte höll sin vanliga högklassiska standard var i situationer då det simulerade materialet var för litet eller att antalet interaktioner var för få. Vid dessa tillfällen så når man dataalgoritmernas upplösningsgräns, som då vanligtvis resulterar i systematiska fel som uppvisar sig som småskaliga eller, i värsta fall, kraftiga fluktuationer i slutresultatet. Dock visade det sig att i de två mer materialrealistiska materialen så reducerades dessa fel och entropin kunde säkert fastställas.

Det var en specifik metod som uppvisade kraftigt avvikande beteenden, som inte berodde på teoretiska felaktigheter beträffande de två entropimetoderna, utan snarare hur värmekapaciteten i sig var beräknad. Utifrån ett teoretiskt underlag så brukar värmekapaciteten beräknas på två sätt, den ena bygger på att fastställa förändringarna i materialets inre energi under små temperaturvariationer via en så kallad derivata, medan den andra metoden utvinner värmekapaciteten utifrån ett mått på hur mycket inre energin varierar och fluktuerar vid en specifik temperatur; ett mått som ofta ses som variansen av energin. Den metod som utnyttjade derivatan producerade de diskuterade godartade resultaten medan det tillvägagångssätt som extraherade värmekapaciteten via variansmetoden frambringade kraftiga fluktuationer som gjorde resultaten totalt obrukbara. Sistnämnt så visade det sig att Metropolisalgoritmen simulerade materialen mer effektivt och precist än Wang-Landaumetoden, som oturligt nog tillförde i vissa fall kraftiga fluktuationer i slutresultatet. Dessutom krävde metoden vissa gånger 25 gånger längre tid att slutföra en fullständig simulation jämfört med den motsvarande Metropolisalgoritmen.

Denna studie har därmed undersökt inom ramarna av de valda metoderna det mest optimala tillvägagångssätt att utföra noggranna simulationsstudier av magnetiska material som uppvisar kraftiga magnetokalorieffekter, och kan i framtiden tjäna som ett vetenskapligt underlag i jakten på denna typ av materialkandidat.

Contents

1 Introduction

The study of magnetic phase transitions has been an active field of research for several decades and still prove to be elusively challenging to describe. Analytical models have been developed to explain the effect, such as the Landau theory of phase transitions[1], but they have unfortunately not been able to completely capture the complex nature of the phenomena. With the ever-improving computer processing power, other sophisticated numerical methods have started to make themselves appreciably fast and accurate in simulating magnetic systems. The numerical take on the problem has gained substantial interest in the hope of achieving precise *ab initio* calculations of the magnetic phenomena which consequently could grant predictive power in developing novel magnetic materials for technological purposes.

Magnetic materials are generally specified by the collective behaviour of their constituent magnetic spins. Collinear alignment of the spins results in a ferromagnetic or anti-ferromagnetic macrostate while non-collinear or canted spin alignment produce more complex magnetic structures. The magnetic phase transition associated with the state change of this magnetic order, e.g from a ferromagnetic to a paramagnetic state, occurs at a certain critical temperature T_c. Varying some intrinsic variable of the system, such as the magnetic field around T_c, one may drive the material to undergo several transitions, flicker between one phase to another. This can give rise to a magnetically driven caloric effect of net cooling or heating, the so-called magnetocaloric effect, since certain thermodynamic quantities are discontinuous and enhanced across these types of phase transitions. In brief, taking a ferromagnet as an example, when an external magnetic field is turned on and the temperature is held constant the magnetic spins align themselves along the field causing an increase in order and thus a decrease in entropy. When the magnetic field is removed the system may relax adiabatically to a state of net decrease in temperature. The reverse is often observed in antiferromagnets which instead give rise to a net heating of the system under the same thermodynamic cycle. In other words, the caloric nature of the material is dependent on its innate magnetic structure. This phenomena has been observed in several rare-earth and transition metal elements and as well in intermetallic alloys[2] though substantial effects have unfortunately only been driven by rather large magnetic fields (up to $3-5T$). This drawback with the material's narrow operating temperature (around its transition temperature) as well as cost of production has so far not made the magnetocaloric effect applicable in commercial devices, thought the prospect of room temperature operating solid state refrigeration is intriguing and may very well be realized in the future[3].

The numerical methods used to simulate the physics of magnetic systems are in many cases based on stochastic processes that mimics the random nature of individual particles but whose collective mean or average reflect the macroscopic properties of the system. This class of numerical methods that utilizes sequences of random numbers to solve problems in e.g statistical physics, fall under the collective name of Monte Carlo methods[4]. One of the many desired quantities that can be computed with the aid of these Monte Carlo simulations is the entropy of the magnetic system. Accurate calculations of the entropy are an important part in identifying the phase stability of the material but also the effective magnitude of the magnetocaloric effect. Discerning the most appropriate method of entropy extraction would take us one step further in realizing an *ab initio* approach in determining effective and consistent novel magnetocaloric materials.

In this paper, a numerical study of the magnetocaloric effect is presented whose main goal is to distinguish and compare two different methods of entropy extraction from magnetic Monte Carlo simulations. In brief, one of the methods derives the change in entropy under a variation of external magnetic field from the order parameter, i.e the magnetization itself. The second method retrieves the entropy change from the field dependent heat capacity of the material. These methods are studied utilizing a minimal spin Hamiltonian consisting of an isotropic Heisenberg model and a Zeeman term. The magnetic systems are simulated with the aid of two different Monte Carlo algorithms, the Metropolis algorithm and the Wang-Landau method, whose effectiveness, accuracy and influence on the thermodynamic properties are discussed in connection with the magnetocaloric results. There are three types of materials that are studied. The first one is a simple cubic toy-model system of only nearest neighbour exchange coupling; whose purpose is to benchmark the entropy extraction methods and to determine the resolution of the two Monte Carlo algorithms. The other two materials are defined via first-principle calculations, thus making them realistic systems in a numerical sense. These consists of a CoMnSi compound and a body centred cubic iron (bcc Fe) magnet, whose purposes are to examine the precision and behaviour of the entropy methods in material realistic systems and to compare the magnetocaloric results with experimental findings.

2 Theory

In this chapter, the theoretical background concerning the thermodynamics of the magnetocaloric effect and the prerequisites of magnetic simulations will be discussed. First, there is an introduction to the physics of thermodynamics and statistical mechanics concerning simple magnetic systems. Necessary theories and quantities are introduced in this section that are expanded upon in the next segment which deals with the magnetocaloric effect itself, including a review of the current state of research in the field. Later on, the intricacies of magnetic interactions are discussed, and the minimal spin Hamiltonian considered in this study, is introduced. Also, the theoretical framework to compute the exchange interactions of the Heisenberg model via a multiple scattering approach is addressed and explained. The last portion of the chapter deals with the topic of Monte Carlo simulations in which the two mentioned algorithms are reviewed and explained in detail.

2.1 Fundamentals of thermodynamics and statistical mechanics

2.1.1 Thermodynamics and magnetic phase transitions

Thermodynamics is a wide branch of physics that deals with the thermal aspects of a system, and its fundamental formulation makes it applicable in several fields of physics and engineering. In short, it considers the possible quantities of a physical process and in a systematic way works out how they are interlinked to each other and how the system's properties are restricted by their action. These quantities are generally divided into two groups, extensive variables that scale with the system such as entropy S, volume V and magnetization M, and intensive variables, independent of the size of the system, which are, for instance, pressure p, temperature T and external magnetic field H. The fundamental principles of thermodynamics can be compiled into four postulates which set the framework of allowed operations. The first postulate assumes that there exists an equilibrium state that is completely characterized by its internal energy U and its intensive and extensive variables. The second one proclaims that in a closed and set equilibrium state, i.e no exchange of e.g particles or energy, there exists a quantity called entropy which is set to be maximized within the constraints of the given variables. The third postulate declares that the entropy is additive of its constituent subsystems, continuous, differentiable and monotonically increasing with respect to energy. Lastly, the fourth postulate dictates that the entropy must vanish at zero temperature[5].

These postulates propose the existence of an abstract quantity, the entropy, which in a broad context is the leading factor that constrains what is permissible or not in a physical process. Determining the entropy is then of significant importance as it reveals a great deal of the state of the system and what kind of operations are admissible. The following discussion will focus on the thermodynamics of a simple magnetic system held at constant volume and pressure with no particle flux.

One of the first steps in quantifying the thermodynamic properties of a magnetic system is to consider the behaviour of the internal energy U, and more precisely, the change in internal energy due to the magnetic work $W = HM$ exerted on the system. The infinitesimal change in U is exactly described by

$$dU = dQ - dW \tag{1}$$

where dQ is the infinitesimal heat absorbed by the system, directly related to its change of entropy via $dQ = TdS$, and $dW = -HdM$ corresponds to the infinitesimal work. It is convenient to introduce other thermodynamic potentials, related to the internal energy via Legendre transformations, such as Helmholtz free energy F, enthalpy E and Gibbs free energy G defined in this case as

$$\begin{aligned} E &= U - MH \\ F &= U - TS \\ G &= U - TS - MH \end{aligned} \tag{2}$$

Differentiating these terms by using the form of Eq.(1) one obtains[6]

$$\begin{aligned} dU &= TdS + HdM \\ dE &= TdS - MdH \\ dF &= -SdT + HdM \\ dG &= -SdT - MdH \end{aligned} \tag{3}$$

These thermodynamic potentials on differential form are exact differentials meaning that, e.g, T can be computed by taking the derivative of U with respect to S while keeping M fixed. Following through all possible derivatives, one acquires the following relations

$$\begin{aligned} T &= \left(\frac{\partial U}{\partial S}\right)_M & T &= \left(\frac{\partial E}{\partial S}\right)_H & -S &= \left(\frac{\partial F}{\partial T}\right)_M & -S &= \left(\frac{\partial G}{\partial T}\right)_H \\ H &= \left(\frac{\partial U}{\partial M}\right)_S & -M &= \left(\frac{\partial E}{\partial H}\right)_S & H &= \left(\frac{\partial F}{\partial M}\right)_T & -M &= \left(\frac{\partial G}{\partial H}\right)_T \end{aligned} \tag{4}$$

Another useful property of exact differentials is that the second derivative is invariant of the order of taking the partial derivatives. This means that in the case of internal energy, the second derivative of U with respect to both S and M can be taken in any order. Applying this feature on the terms in Eq.(4) one obtains four Maxwells relations on the form[7]

$$\left(\frac{\partial T}{\partial M}\right)_S = \left(\frac{\partial H}{\partial S}\right)_M \quad (5), \qquad \left(\frac{\partial T}{\partial H}\right)_S = -\left(\frac{\partial M}{\partial S}\right)_H \quad (6), \qquad \left(\frac{\partial S}{\partial H}\right)_T = \left(\frac{\partial M}{\partial T}\right)_H \quad (7), \qquad \left(\frac{\partial S}{\partial M}\right)_T = -\left(\frac{\partial H}{\partial T}\right)_M \quad (8)$$

These Maxwells relations show how these variables are connected to one another, in maybe seemingly unrelated ways. They also put constraints on the properties that can be acquired from the system, e.g keeping the magnetic field constant at all times forces the temperature and entropy in certain circumstances to be fixed with respect to magnetization. Another interesting upshot of the Maxwells relations is that indirect measurements of the entropy becomes possible via measurements of the magnetization held at constant magnetic field. This feature will be a central topic in this study and will be further touched upon in section 2.2 where the magnetocaloric effect is described in detail.

It is highly practical to introduce a response function called the heat capacity which is a quantity that reflects the system's capability to absorb heat with respect to changes in temperature. It is defined as

$$C_x = \left(\frac{\partial Q}{\partial T}\right)_x = T\left(\frac{\partial S}{\partial T}\right)_x \tag{9}$$

in which x indicate what variable is held constant. In this magnetic system, two heat capacities can be identified, C_M in which the magnetization is kept fixed and C_H where the field is constant. Using Eq.(9) and Eq.(3) one obtains C_M and C_H as

$$C_M = T\left(\frac{\partial S}{\partial T}\right)_M = \left(\frac{\partial U}{\partial T}\right)_M = -T\left(\frac{\partial^2 F}{\partial T^2}\right)_M \tag{10a}$$

$$C_H = T\left(\frac{\partial S}{\partial T}\right)_H = \left(\frac{\partial E}{\partial T}\right)_H = -T\left(\frac{\partial^2 G}{\partial T^2}\right)_H \tag{10b}$$

where the last equality comes around due to the relations of Eq.(4). Another response function that is widely used is the magnetic susceptibility which gives a quantitative description of what kind of influence a variation in magnetic field has on the magnetization of the system. It is defined as

$$\chi_x = \left(\frac{\partial M}{\partial H}\right)_x \tag{11}$$

which with the relations of Eq.(4) result in two types of susceptibilities, one of constant temperature and one with constant entropy[6]

$$\chi_T = \left(\frac{\partial M}{\partial H}\right)_T = -\left(\frac{\partial^2 G}{\partial H^2}\right)_T \tag{12}$$

and

$$\chi_S = \left(\frac{\partial M}{\partial H}\right)_S = -\left(\frac{\partial^2 E}{\partial H^2}\right)_S \tag{13}$$

The thermodynamic relations presented here serves as a foundation in quantifying and calculating the thermodynamic properties of magnetic materials. However, magnetic phase transitions have proven to be elusively difficult to describe as they bring forth abrupt changes and discontinuities in the mentioned thermodynamic quantities. One of these properties that are altered across a phase transition is the non-zero order parameter, i.e magnetization M, which defines the ordered phase of a magnet below some critical transition temperature. When the temperature rises above the critical temperature, the magnetization vanishes, and the system becomes paramagnetic with no preferred magnetic orientation. This means that at the critical point the phase transition alters the state of the system and its thermodynamic properties, which can happen in either a smooth or disrupt fashion. The nature of the transition can be classified as either a first-order transition, in which the first derivative of the free energy is discontinuous (i.e the magnetization M), or a second-order transition in which it is the second derivative of the free energy that is discontinuous (e.g the susceptibility χ). The specific value of the critical temperature is a material specific quantity which is constant if no external stimuli are present, but under the influence of e.g a magnetic field, the value is not fixed but rather a function of the applied field. For ferromagnets, the transition temperature generally increases monotonously with field strength while it the opposite for antiferromagnets[8]. Mapping the corresponding critical temperature values one can compile phase diagrams portraying the set of variable values that trigger a transition.

The abrupt changes in these thermodynamic quantities give rise to interesting consequences, e.g enhancements in the magnetocaloric effect which will be discussed in section 2.2.

2.1.2 Statistical mechanics

Statistical mechanics is a powerful and, in many cases, necessary tool that circumvents the problematic and often unsolvable equations of motion that arise in a classical description of a many-body problem and instead approaches the matter in a stochastic fashion. Here, the system is quantified in terms of its possible microstates, a representation of all the system's attainable phase space configurations. This means that a specific microstate corresponds to a particular state of the

system, which in turn implies that the whole set of microstates completely describes the system of interest. Allowing the energy of the system to span an arbitrarily large range of energy levels, following the so-called canonical formalism, leads to the conclusion that some states are less likely to occur than others at thermal equilibrium. This means that it is justifiable to prescribe a finite probability to each of these microstates such that they precisely reflect the probability to find the system in a specific state with energy E. This means that their collective behaviour, averaging all the possible configurations, should mirror the observable macroscopic properties of the system[5].

The probabilistic nature of these microstates enables physicists to tackle the problem in a completely new manner, and the theory has flourished since the early 1900s. It was at this early time that the microstates got a physically suitable probability distribution, the so-called Boltzmann distribution, which depend on the energy of the microstate and the system's equilibrium temperature. A central quantity that is derived using the Boltzmann distribution and contains all the information of the microstates is the partition function

$$Z = \sum_{\text{All microstates}} e^{-\frac{\mathcal{H}}{k_B T}} = \sum_{\text{All microstates}} e^{-\beta \mathcal{H}} = \sum_{E} g(E) e^{-\beta E} \tag{14}$$

in which k_B is the Boltzmann constant, $\beta = (k_B T)^{-1}$, $\mathcal{H}$ is the Hamiltonian describing the system of interest with corresponding energy eigenvalue E and $g(E)$ is the density of state at that particular energy level. The partition function is summed over all possible microstates of the system, meaning that it scales with its size and the degrees of freedom per interacting particle.

The last equality in Eq.(14) represents a more appropriate way to calculate the partition function. Here, the sum covers all the energy levels of the system instead of the more abstract notion of microstates, though it retains the energy state degeneracy by weighting the distribution with the density of states, which essentially is a measure of the number of states per energy level. With this at hand, one can define the probability that the system is found in a specific state as

$$\mathcal{P}_\mu = \frac{g(E_\mu) e^{-\beta E_\mu}}{Z} \tag{15}$$

where E_μ corresponds to the energy output of the Hamiltonian in the state μ. Continuing using the tools of statistics, one can write down an expression for the expectation value of an observable quantity Q by summing up its contribution per microstate and weighting it with its corresponding probability

$$\langle Q \rangle = \sum_\mu Q_\mu \mathcal{P}_\mu = \frac{1}{Z} \sum_\mu Q_\mu g(E_\mu) e^{-\beta E_\mu} \tag{16}$$

In the case of the expectation value of the Hamiltonian, i.e $\langle E \rangle$, one may exploit the exponential form of the partition function to specify $\langle E \rangle$ in terms of a partial derivative of Z with respect to β, i.e

$$U = \langle E \rangle = -\frac{1}{Z} \frac{\partial Z}{\partial \beta} = -\frac{\partial \log Z}{\partial \beta} \tag{17}$$

Here the energy expectation value has been noted to correspond to the internal energy U due to the fact that the Hamiltonian itself encompasses all the interactions of interest leading to a full coverage of all the energy configurations of the system. This in turn implies that it should be possible to describe the system's internal energy in terms of the expected occupation of energy levels, namely $\langle E \rangle$. A consequence of this notion is that the magnetic work, e.g Zeeman interaction, can be implicitly included in the internal energy, resulting in no explicit work terms in the thermodynamic equations of Eq.(3). This means that the differential form of U in Eq.(1) will be exactly equal to the infinitesimal change in heat dQ, which in turn makes the heat capacity uniquely specified by the derivative of U with respect to T regardless of the form of the Hamiltonian. Here one may also notice that the statistical mechanics approach also eliminates the need to fix M or H in order to specify a heat capacity; the two definitions of Eq.(10) are in this formulation equivalent. Relabelling it as C, statistical mechanics defines the heat capacity as

$$C = T \left(\frac{\partial S}{\partial T} \right) = \frac{\partial U}{\partial T} = k_B \beta^2 \frac{\partial^2 \log Z}{\partial \beta^2} \tag{18}$$

where the last equality follows from the form of Eq.(17). An interesting consequence of the particular form of U is that the energy fluctuations, i.e its mean square deviations, are related to the heat capacity itself. By using Eq.(16-18) one obtains the following alternative form of the heat capacity

$$\langle (E - \langle E \rangle)^2 \rangle = \langle E^2 \rangle - \langle E \rangle^2 = \frac{\partial^2 \log Z}{\partial \beta^2} = \frac{C}{k_B \beta^2} \tag{19}$$

The magnetic susceptibility of Eq.(11) can in a similar fashion as the heat capacity be related to the fluctuations of the magnetization itself, taking on the form

$$\chi = \beta \left(\langle M^2 \rangle - \langle M \rangle^2 \right) \tag{20}$$

Another useful quantity that can be computed from Eq.(18) is the entropy, which is obtainable after integration with respect to temperature. Using the fact that the entropy should vanish at zero temperature to remove possible integration constants the result becomes

$$S = -k_B \beta \frac{\partial \log Z}{\partial \beta} + k_B \log Z \tag{21}$$

The equations outlined in this section show how the previously defined thermodynamic quantities can be calculated within this new stochastic approach. Here, one may notice that all thermodynamic properties are connected to the partition function itself, meaning that if the partition function is known, then all features of the system can be extracted from its notion. Unfortunately, complete knowledge about this quantity is rare to find, though a numerical method that computes the density of states, necessary in the calculation of the partition function, is discussed in section 2.4.

2.2 The magnetocaloric effect

The first scientific reports on the Magnetocaloric effect dates back to 1917 from an experimental study by P. Weiss and A. Pickard[9]. They discovered a slight temperature change in nickel while varying a magnetic field close to its magnetic phase transition temperature, indicating the existence of a caloric effect of purely magnetic nature. In the 1920s, P. Debye[10] and W. F. Giauque[11] independently suggested a process that could effectively cool substances down to sub-kelvin degrees by repentantly demagnetize certain paramagnetic salts. This was later realized in 1933 by W. F. Giauque and D. P. MacDougall[12] where they attained a temperature of $0.25K$ in gadolinium sulphate, $Gd_2(SO_4)_8H_2O$, and the technique has since then been frequently used to cool matter down to very low temperatures. On the other hand, the compelling possibility of room temperature refrigeration based on the magnetocaloric effect soon started to be investigated, and in 1976, G. V. Brown and S. S. Papell[13] showed that gadolinium, Gd, with a transition temperature of $294K$, could be used to accomplish a net cooling with the aid of an alternating magnetic field of about $7T$ in strength. This was the first step in an extensive scientific pursuit of finding magnetic materials exhibiting substantial magnetocaloric properties whilst being operational at room temperature conditions[3]. In this section, we will dive deeper into the physics and research of the magnetocaloric effect to depict its underlying mechanism and showcase the ideas of magnetic cooling devices.

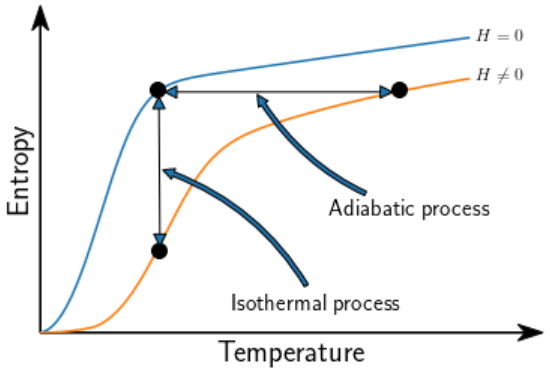

Figure 1: Illustration of the magnetic entropy under the presence and absence of an external magnetic field. The isothermal and adiabatic processes indicated here emphasize the enhanced entropy and temperature change between these two descriptions.

The thermal response that some magnetic materials display whence affected by an external magnetic field is commonly caused by the interplay between the magnetic moments and the vibrational modes of the atomic lattice. It all emerges due to the conservation of the system's total entropy under adiabatic conditions, i.e the full entropy stays constant before and after a variation of some intensive or extensive variable. Keeping in mind that the system's degrees of freedom are embedded in terms of the electrical, lattice (phonon) and magnetic contributions suggest that the total entropy should be composed of the individual entropies related to these subcategories. When the volume and pressure are held constant, the premise is that the full entropy is merely a function of temperature and external field. Putting this all together we obtain

$$S(T, H) = S_m(T, H) + S_{El}(T, H) + S_{Lat}(T, H) \tag{22}$$

where S_m, S_{El} and S_{Lat} are the magnetic, electronic and lattice entropy contributions respectively. In most cases, the field dependency of the electronic and lattice entropies is negligible compared to the magnetic part. This means, to a large extent, that if a magnetic field is applied isothermally only the magnetic entropy is affected and altered. In the case of a ferro or paramagnet, the moments tend to align with the field which in turn causes the system to be more structured, thus reducing the magnetic and total entropy by an amount $|\Delta S|$ which is the difference in total entropy before and after the change in field at constant temperature. Removing the magnetic field under adiabatic conditions forces the temperature to be lowered due to the fact that the temperature is the only free parameter in the entropy function and the third postulate of thermodynamics dictates a reduction in thermal energy in relation to the previous entropy change $|\Delta S|$. This shows up as a decrease in the vibrational energy of the lattice which lowers the system's overall kinetic energy, and thus also its temperature. So, the conservation of entropy before and after field removal induces a net cooling of the system that is purely driven by a thermodynamic cycle of isothermal and adiabatic variation of an external field. The reverse is usually observed in antiferromagnets as magnetic fields tend to force the magnet's oppositely oriented moments to a less ordered

canted state which in turn leads to an increase in entropy. This would make the thermodynamic cycle discussed above end up heating the material instead of cooling it. The magnetic materials that exhibit these properties have what is called an inverse magnetocaloric effect, while those of the first category are named the conventional type.

The change in entropy and temperature can be enhanced in a region close to a phase transition as some of the thermodynamic quantities are discontinuous from one phase to another. This peculiarity can be exploited with the fact that the critical temperature is not a fixed quantity, but instead rather malleable, and can be shifted to higher or lower values with the aid of an external field, as discussed in section 2.1.1. This means that the temperature in the isothermal part of the cycle can be chosen in such a way that it lies in between the two transition temperatures occurring with and without the presence of the field. At this particular point, the two entropy descriptions, i.e $S(T,0)$ and $S(T,H)$, exhibit dissimilar behaviour, with one being in the ordered state while the other, disordered. When the field is applied, it drives the system to transfer from one phase to another, significantly amplifying the entropy change as illustrated in Fig. 1. This enhancement produces an even greater effective temperature variation per thermodynamic cycle, increasing the overall efficiency and usefulness. Hence, to produce optimal performance, the magnetic material itself should exhibit both large entropy and temperature alterations while at the same time have an inherent transition point close to room temperature to make use of this highly desired caloric quality.

In these processes, entropy is evidently a central quantity that governs the effectiveness of the caloric cycle, and thus also the total induced temperature change. One way of obtaining the entropy stems from the Maxwell relation of Eq.(7), which after integration with respect to field becomes

$$\Delta S = \Delta S(T, 0 \to H) = \int_0^H \left(\frac{\partial M}{\partial T}\right)_{H'} dH' \tag{23}$$

This equation connects the magnetic entropy change with the combined rate of change of the magnetization with respect to temperature over the full interval of the applied field. The derivative in this expression becomes discontinuous in a second order phase transition, as discussed in section 2.1.1, which in turn can produce a peaked behaviour in ΔS close to the material's innate transition temperature. Another way of computing the change in entropy comes from statistical mechanics and more precisely Eq.(18). Here, after integration with respect to temperature, the equation shows that the entropy at temperature T and field H is given by

$$S(T,H) = S_0 + \int_0^T \frac{C(T',H)}{T'} dT' \tag{24}$$

where S_0 correspond to an integration constant and can generally be taken to be zero as the fourth postulate of thermodynamics affirms that the entropy should vanish at absolute zero. The contribution of the magnetic field is implicitly included in the heat capacity which makes it possible to determine the field induced isothermal change in entropy, i.e $\Delta S(T, 0 \to H)$ as

$$\Delta S = \Delta S(T, 0 \to H) = S(T,H) - S(T,0) = \int_0^T \frac{C(T',H) - C(T',0)}{T'} dT' \tag{25}$$

The change in entropy is in this case computed as the temperature cumulative difference of heat capacities in the presence and absence of field. The integrand will in a similar fashion to the previous ΔS formula show a peaked behaviour under a second order phase transition due to the fact that the second order derivative of Eq.(10) is discontinuous.

The two equations of isothermal entropy variation presented here offer two distinctly different ways to measure and compute the system's change of entropy. The first equation, Eq.(23), require direct measurement of the magnetization under varying field strength at different temperature steps, experimentally achievable via e.g superconducting quantum interference devices (SQUID) magnetometry[14]. While on the other hand, varying the same set of variables, caloric measurements of the heat capacity via e.g differential scanning calorimetry (DSC)[15] enable indirect determination of the change in entropy via the second equation, Eq.(25). Computation of the magnetization and the heat capacity via numerical simulation will be of a completely different matter as the models used to simulate the magnet constrain and limits the system via e.g approximations, finite systems or even the extent of the models themselves. The extraction of the two discussed entropy variations via numerical simulations is, therefore, the central part of this study, and its specifics are discussed throughout the paper.

Knowledge about these two expressions makes it possible to indirectly ascertain the material's adiabatic temperature change, by first noting that the entropy itself is a function of only temperature and field, which means that its exact differential will be of the form

$$dS = \left(\frac{\partial S}{\partial T}\right)_H dT + \left(\frac{\partial S}{\partial H}\right)_T dH \tag{26}$$

Relating the two terms of the right hand side with the form of Eq.(18) and Eq.(7), the entropy differential becomes

$$dS = \frac{C}{T}dT + \left(\frac{\partial M}{\partial T}\right)_H dH \tag{27}$$

Here, as it is the adiabatic process of the thermodynamic cycle that is considered, the infinitesimal change in entropy is per definition zero, $dS = 0$. With this in mind, rearranging the terms of Eq.(27) and integrating, one obtains the adiabatic temperature change as

$$\Delta T = \Delta T(T, 0 \to H) = -\int_0^H \frac{T}{C(T,H')}\left(\frac{\partial M}{\partial T}\right)_{H'} dH' \tag{28}$$

This formula enables indirect measurements of the effective temperature change per thermodynamic cycle, but it requires both of the aforementioned quantities of magnetization and heat capacity as functions of both field and temperature to be computed. Experimental direct measurements, via temperature sensors, give a straightforward indication of the material's actual performance, circumventing the need to map out the results of M and C with respect to field and temperature[3].

The scientific investigation concerning the materials exhibiting substantial magnetocaloric effect is an extensive, active and continuously growing field of research, and too large to be justifiably reviewed in this paper. A brief and general summary of the materials that demonstrate the phenomena will instead be presented in order to still capture the overall development in the field. Discussing the findings will make way to the final topic of the magnetocaloric section which is a short summary of the basic concepts of refrigeration devices and their inner workings. A thorough and comprehensive review of the experimental findings and methodologies can be read in the paper written by V.Franco and co-workers of Ref.[16], Ref. [3] written by M. Bali *et al* and Ref.[17] by J. Lyubina.

Generally, all sorts of magnetic materials display some sort of magnetocaloric effect, but usually only in minute amounts. Substantial magnetocaloric properties are rather rare, but even rarer are the ones that have a transition temperature around ambient temperature. The materials manifesting these attributes can predominantly be grouped into classes and families of crystalline or amorphous compounds and alloy. An intriguing feature of alloying with different elemental compositions and concentrations is the possibility to tailor the transition temperature of the material and its magnetic properties to be suitable for a specific purpose. One of the largest groups of these materials, and the one that has gained the most interest, is gadolinium related alloys. The rare earth element itself possesses exceptionally large magnetic moments, about $\sim 7.5\mu_B$ per atom, and exhibit significant magnetocaloric properties around $294K$, even on its own[2]. This insinuates that a number of alloys doped with gadolinium should showcase similar caloric qualities, which has been observed in e.g $Gd_{1-x}Dy_x$, $Gd_{1-x}Tb_x$, Gd_xHo_{1-x}, $Gd_{1-x}Y_x$ and $Gd_5Si_2Ge_2$ in which the x label corresponds to the concentration in percent of the elements. Many of these alloys display a broadening in the operational temperature in contrast to pure gadolinium making the refrigeration process more flexible. Another distinguishing feature of the gadolinium-based materials is the small hysteresis losses, meaning that the loss of thermal energy due to the realignment of the moments under varying field is negligibly low. Altogether, the gadolinium alloys are often regarded as the benchmark and reference prototype in the development of effective refrigeration devices, but unfortunately, they are not expected to be relevant when it comes to upscaled mass productions due to the high cost of the rare earth elements.

Another promising class of materials is the lanthanum-based compounds, more precisely, $La(Fe_xSi_{1-x})_{13}$ compositions, which can also be appended with e.g hydrogen, carbon and cobalt for an even broader range of features. Even though lanthanum is a rare earth element, the stoichiometric composition of the compound allows for fewer lanthanum atoms per unit cell compared to the mentioned gadolinium alloys. With the abundance of the other constituent elements, the La-Fe-Si compounds become an affordable candidate for mass-produced refrigeration devices. This class of material produces comparable results to the gadolinium-based ones, with adiabatic temperature changes reaching, for example, $\Delta T \sim 15.4K$ measured in a $La(Fe_{0.9}Si_{0.1})_{13}H_{1.1}$ crystal at $287K$ under the variation of a magnetic field of $5T$[18]. A drawback with these compounds is that without proper production preparation, i.e annealing at high temperatures for up to weeks at length, the materials become quite brittle and difficult to handle. An interesting upshot of this is that the materials are manufactured as grains or flakes instead of the conventional blocks or sheets which reduces the mechanical stress and increases the surface to volume area, an important factor to consider in the actual refrigeration prototypes[3].

Some manganese and iron-based compounds, e.g $MnFeSi_xP_{1-x}$, $MnFeP_{1-x}As_x$ and $MnFeP_{1-x}Ge_x$ also show very attractive caloric properties in ambient conditions. The compounds containing arsenic show excellent adiabatic temperature changes, up to $\Delta T = 9.8K$ for $MnFeP_{45}As_{55}$ at $308K$ for $\Delta H = 5T$[19], but the toxicity of arsenic must be taken into consideration in domestic devices. Substituting arsenic with silicon or germanium still retains equivalent caloric qualities of the compounds, though at the cost of increased hysteresis losses, which in certain circumstances can be remedied with the addition of boron[17].

Magnetic materials exhibiting magnetocaloric effects						
MC material	T[K]	$\lvert\Delta S\rvert$[J Kg^{-1} K^{-1}]	$\lvert\Delta S\rvert$[J mol^{-1} K^{-1}]	$\lvert\Delta T\rvert$[K]	ΔH[T]	Reference
Gd	294	11	1.73	13^{d}	5	20
$Gd_5Si_2Ge_2$	280	19	2.08	15^{i}	5	20
$La(Fe_{0.88}Si_{0.12})_{13}$	195	23	1.35	8.6^{i}	5	21
$La(Fe_{0.9}Si_{0.1})_{13}$	184	30	1.77	12.1^{i}	5	21
$La(Fe_{0.9}Si_{0.1})_{13}H_{1.1}$	287	31	1.84	15.4^{i}	5	18
$Mn_{1.24}Fe_{0.71}P_{0.46}Si_{0.54}$	320	12	0.55	3.0^{i}	1	22
$MnFeP_{0.45}As_{0.55}$	308	18	0.99	9.8^{i}	5	19
CoMnSi	250	6.5	0.31	1.7^{d}	5	23
$Ni_{52.6}Mn_{23.1}Ga_{24.3}$	300	18	1.09	12^{i}	5	24
$Ni_{55}Mn_{20}Ga_{25}$	311	29	1.76	2.2^{d}	5	25
$Ni_{45.2}Mn_{36.7}In_{13}Co_{5.1}$	317	18	1.16	6.2^{d}	2	26
$Ni_{50}Mn_{37}Sn_{13}$	299	18	1.17	12^{i}	5	27

Table 1: A selection of magnetic materials exhibiting substantial magnetocaloric properties. The temperature of the isothermal measurements is denoted as T, the isothermal entropy change correspond to ΔS, the adiabatic temperature change as ΔT and the complete variation of magnetic field is represented as ΔH. The superscripts i and d correspond to results obtained via indirect or direct measurements respectively.

The last family of materials that will be assessed is the Heusler alloys. This group of materials is stoichiometry defined by the formula X_2YZ in which X corresponds to some transition metal element, Y being either transition, rare-earth or alkaline rare-earth and Z represent an element from the p-block. X corresponds in many cases to nickel of the 3d transition elements but can be chosen to be, for example, iron, cobalt and platinum. The Y component is usually the constituent that induces the alloy's magnetic properties on its own or in union with the X component and is often times chosen to be manganese. Lastly, gallium, indium, tin or antimony has shown to be common elements taking the place of the Z atom in the formula. The substantial magnetocaloric effects that can be found in a number of these alloys are mainly contributed by a structural phase transition coinciding with the magnetic phase transition. This conjoined transition boosts the caloric property of the material to significant values, almost comparable to the previously mentioned categories[16]. Unfortunately, the reliance on the structural phase transition causes the Heusler alloys to be rather volatile as it is common that the first thermodynamic cycle results in an agreeable temperature change while subsequent magnetic field variations only produce a fraction of the effect. An example of this principle can be seen in $Ni_{45}Mn_{37}In_{13}Co_5$ examined in the temperature interval $313K \leq T \leq 321K$ under the field variation $\Delta H = 1.9T$ from Ref.[17]. The first cycle produced an adiabatic temperature change of about $|\Delta T| \sim 4.3K$ while the second and succeeding field variations only induced a change of about $|\Delta T| \sim 1.3K$. This is attributed to the magnetically difficult or inconceivable task of returning the structure to its starting configuration for each repetition of the cycle. This means that after the first field variation, the crystal structure and its magnetism are altered from the material's initial state and can only be returned to its original configuration by annealing or being subjected to a very strong magnetic field $\sim 10T$. Another inconsistency of the measured magnetocaloric properties of the Heuseler alloys is the discrepancy between direct and indirect measurements of the thermodynamic quantities. The rather large difference in $|\Delta T|$ in Ni-Mn-Ga alloy measurements can be taken as an example. Here, indirect measurements of $Ni_{52.6}Mn_{23.1}Ga_{24.3}$ from Ref.[24] showed a temperature difference of $12K$ while a similar composition of $Ni_{55}Mn_{20}Ga_{25}$ from Ref.[25] showcased a directly measured temperature difference of $2.2K$. The disagreeing results are unlikely caused by the minuscule dissimilarities of the alloy compositions. A more plausible explanation would be that the adiabatic temperature change formula of Eq.(28) has been wrongfully misused. Since the Maxwell relations, which were determined on the premise of no volume or lattice contributions, have been directly implemented in the derivation of Eq.(28), causes the formula to disregard any effects related to structural alterations. This gives rise to artifact remnants when computed, which in turn causes an exaggerated final result[16]. These primary features make the Heusler alloys as a category improbable candidates for effective magnetocaloric devices.

Table 1 displays a selection of magnetic materials and their magnetocaloric properties from the mentioned classifications. As been previously discussed, the isothermal entropy and adiabatic temperature change give a considerable indication of the absolute effectiveness of the material, but these values are not the only contributing qualities to have in mind when developing refrigeration devices. Cost of production, thermodynamic reversibility, operation temperature, hysteresis losses, brittleness, corrosion and heat dissipation properties are but some complementary factors to consider in this scheme. Another central aspect to reflect upon is the heat exchange itself between the caloric material and, usually, a heat transfer fluid. The fluid serves as a heat dissipation medium that is either heated or cooled during the thermodynamic cycle, which after completion is carried away from the magnet. The transferred heat from cycle to cycle can then be merged into a net cooling channel, constituting the overall net cooling effect of the refrigeration device. Here, the addressed grain or flake structures are excellent designs in the regard that the contact area between the magnet and the heat transfer fluid is greater compared to the more conventional stacked sheet shapes. This facilitates the heat exchange in such a way that

a decrease in the lag time can be observed between completion of the thermodynamic cycle and temperature equilibration of the two mediums. The compatibility between the magnet and the heat transfer fluid becomes an important matter as the risk of oxidation or corrosion would render the caloric material useless, and with it, a short-lived refrigeration device. The inclination of these effects differs from magnet to magnet and a protective coating could very well be necessary in order to shield the magnetic material from direct contact with the fluid.

The source of the magnetic field has also been a topic of discussion; whether to use super strong permanent magnets or a wired electromagnet, pulsed on and off by an alternating electric current. The requirement of very strong magnetic fields is still one of the biggest drawbacks of the magnetocaloric effect, and the absolute output of the entropy and temperature change scale with the strength of the applied field. The alternative of an electromagnetic source, i.e an electromagnet, that can be pulsed on and off is an appealing option as the field strength can be tuned by simply varying the magnitude of an electric current. Unfortunately, electromagnets have proven to be highly energy inefficient due to excessive heat productions in the form of Joule heating in the coils of the electromagnet. Permanent magnets, on the other hand, circumvent these deficiencies but are at the same time limited in the sense that they can only produce fields up to $\sim 2T$ in strength, achievable via e.g Fe-Nd-B permanent magnets. Improved capacities can be obtained by the use of superconducting magnets which can push the absolute field strength to higher order values, making the overall refrigeration more effective. Though, the generally low operation temperature of superconducting magnets makes magnetocaloric devices based on this source unlikely to make their way into domestic environments and might only be useful for large industries. The variation of the field itself is made possible by either mechanically moving the permanent magnet or the magnetocaloric material in and out of range of the magnetic field[16].

2.3 Effective Heisenberg spin Hamiltonian and the LKAG method

Some magnetic materials experience a spontaneous magnetic ordering below a critical temperature; the so-called Curie temperature T_c in the case of ferro- or ferrimagnets and Néel temperature T_N for antiferromagnets. When temperatures rise above the critical temperature, the orientation of the magnetic moments suddenly becomes random triggering the magnet to behave like a paramagnet. The mechanism behind spontaneous magnetic ordering is completely quantum mechanical in its nature and its fundamental description stems from the Pauli exclusion principle which states that two identical fermions cannot occupy the same quantum state. This causes the electrons in a many-body system, like in a solid, to have a collective wavefunction that is antisymmetric under the interchange of two electrons. Since the typical non-relativistic electronic Hamiltonian, or molecular Hamiltonian under Born-Oppenheimer approximation, describing the multitude of Coulomb interactions between electrons and nuclei is spin independent, the total electronic wavefunction must be a product of a spatial part governing the coordinates of the electrons and a spin part containing the spin information of the electrons. The antisymmetry of the wavefunction constrains the spin and spatial states in such a way that in some cases a spin-dependent splitting of energy eigenvalues occurs which in turn results in an energetically preferred spin orientation[28]. This mechanism gives an explanation of why spontaneous magnetic order can occur and its close relationship with the interchange of spins has given it the name exchange interaction.

Focusing on an explicit formulation of the phenomena, the indirect spin-dependency of the electronic Hamiltonian makes it possible to detach the spin degrees of freedom in such a way that an effective spin Hamiltonian that only takes the exchange interactions into account can be constructed. Unfortunately, due to its complexity, only approximate models have been developed which are, in general, only representative for particular classes of magnets. One of the most famous models of magnetism is the Heisenberg model which relies on the existence of localized magnetic moments which interact with each other via exchange interactions. By also taking magnetic fields into consideration, the effective spin Hamiltonian will be of the form

$$\mathcal{H} = -\sum_{i \neq j} J_{ij} \boldsymbol{m}_i \cdot \boldsymbol{m}_j - \boldsymbol{H} \sum_i \boldsymbol{m}_i \tag{29}$$

where the first term corresponds to the Heisenberg model which pairwise couples the magnetic moments $\boldsymbol{m}_i$ and $\boldsymbol{m}_j$ via the exchange coupling parameter J_{ij} while the second part is called a Zeeman term in which every magnetic moment interacts with a magnetic field $\boldsymbol{H}$. Without an external field, the sign and strength of J_{ij} determine the ground state configuration of the moments. A positive nearest neighbour coupling orients the moments parallel to each other while a negative signed nearest neighbour J_{ij} align the moments in a canted or antiparallel fashion depending on the symmetry of the lattice. The coupling itself can be of a direct nature where the moments' wavefunctions overlap and affect each other directly according to Pauli's principle. The moments may also interact with each other through indirect coupling in which the exchange is mediated between moments via an intermediate particle, like an electron, which simultaneously couples to both of the paired localized moments. The indirect exchange coupling that is mediated via mobile conduction electrons is known as the Rudermann–Kittel–Kasuya–Yosida (RKKY) interaction[29,30,31] and it shows how even well-separated moments can influence each other and give rise to magnetic order. An interesting feature of the RKKY interaction is that the coupling strength exhibits a damped oscillatory behaviour, dropping off with distance and fluctuating between positive and negative signed values.

This means that the interaction is quite long ranged, but at certain distances, the coupling is of ferromagnetic nature while at other coordinates it is instead antiferromagnetic[32].

In order to make use of the model and make the system material specific, the determination of the coupling constant J_{ij} is of paramount importance. This has proven to be no easy task, but one method proposed in 1987 by Lichtenstein and co-workers, currently known as the LKAG method[33], was successful in developing a formula that interlinked electronic structure calculations with the exchange parameter, meaning that self-consistent *ab initio* determination of J_{ij} could be realized. The general idea behind this procedure is that an infinitesimal rotation of two magnetic moments at site i and j in a collinear ferromagnetic ground state will cause an energy variation in the Heisenberg model proportional to the exchange parameter J_{ij} and the two angle rotations as well. At the same time, looking into the problem of two infinitesimal rotations from a multiple scattering point of view, following a similar formalism as the Korringa, Kohn and Rostoker (KKR) Green function method[34], one may derive a total energy variation that is proportional to a prefactor and, similarly, the two angle rotations. Relating the exchange parameter with this prefactor one ends up with the LKAG formula

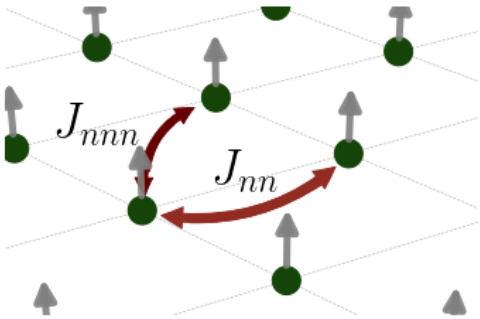

Figure 2: Figurative illustration of the nearest neighbour J_{nn} and next nearest neighbour J_{nnn} exchange coupling in a ferromagnetic simple cubic environment.

$$J_{ij} = \frac{1}{\pi} \int_{-\infty}^{\epsilon_F} d\epsilon Im\Big[Tr_L(p_i T_{ij}^{\uparrow} p_j T_{ji}^{\downarrow})\Big] \tag{30}$$

where ϵ_F is the Fermi energy, p_i is the spin-dependent inverse single site scattering operator (ISO) evaluated at site i, $T_{ij}^{\uparrow}$ ($T_{ij}^{\downarrow}$) is the scattering path operator (SPO) governing the scattering process between site i and j in the collinear spin-up (spin-down) channels and the trace runs through the orbital space comprised of both angular and magnetic quantum numbers $L = (l, m)$. Full derivations of the formula can be found in the original paper of Ref. [33] .

Looking closer into Eq.(30) to deduce the meaning of the individual components and how J_{ij} can be obtained from electronic structure calculations one may start off disclosing the nature of the ISO and SPO. In brief, multiple scattering theory relies on the indefinite and subsequent scatterings of electron waves, propagating from one scattering event to the next. The single site scattering operator, $t_i = p_i^{-1}$, describes a single scattering event occurring at site i which is governed by its local potential V_i, while the SPO of both the spin-up and spin-down channels

$$\tau_{ij} = \begin{pmatrix} T_{ij}^{\uparrow} & 0 \\ 0 & T_{ij}^{\downarrow} \end{pmatrix} \tag{31}$$

describes the scattering process between site i and j. In other words, the SPO is described by an infinite Dyson series of single-site scatterings, meaning that the SPO is a sum of all possible scattering paths that can occur going from site i to site j. This is neatly formulated as[35]

$$\tau_{ij} = t_i \delta_{ij} + t_i G_0 \sum_{k \neq j} \tau_{kj} \tag{32}$$

where G_0 is the system's free Green function, which is viable in the interstitial regions between sites where the electrostatic potential is more or less flat, following the so-called muffin-tin approximation. This gives the free Green function the interpretation of a propagator function, which propagates the scattering particle from one site to the other, interlinking the multitude of scattering events between site i and j in Eq.(32). In order to determine the SPO, the scattering process at each local site must first be established and computed. In other words, the single site scattering operator t_i governing this process, expressed as[36]

$$t_i = \frac{1}{V_i^{-1} + G_0} \tag{33}$$

is a key quantity of this formalism. With these equations at hand, the exchange parameter J_{ij} can be readily determined if the atomic local potential V_i and the Green function G_0 is known for the system of interest. There are many different ways to properly determine the values of V_i and G_0, and the interested reader can find a full description on the topic and a more extensive explanation of the multiple scattering method in Ref. [37]. Though generally, self-consistent electronic structure calculations are the most commonly used procedure as many ground state properties, including the atomic potentials V_i, can be extracted from the solid.

The LKAG method has since its appearance given physicists a proper justification to implement effective spin models to research the magnetic interactions of magnets by making the exchange parameter material specific. Not only that, but the method has also shed some light on the promise of accurate *ab initio* calculations of magnetic properties. Regrettably, the method comes with a couple of limitations. One of the main flaws is that it assumes a collinear, often ferromagnetic, initial ordering, neglecting non-collinear and canted orientations. Another limitation is that it does not include spin-orbit coupling which becomes increasingly relevant in e.g rare-earth elements and thin-film systems where relativistic effects are non-negligible[38]. In 2017, a theory of non-collinear exchange interactions was proposed by A. Szilva and co-workers[39] in which they showed that the energy variations derived from a multiple scattering formalism could rarely be fully mapped onto a Heisenberg exchange parameter alone. It was shown that, more often than not, the expression came with an extra term, which meant that there was no longer a one-to-one procedure of computing J_{ij}, except in the particular case of collinear systems in which the LKAG formula could be retrieved. This mismatch implies that even ferromagnets, studied at finite temperatures where the magnetic structure starts to deviate from the collinear ground state, are not completely described by the Heisenberg model alone, only approximately. A. Szilva and co-workers also showed in 2013[40] that the Heisenberg exchange parameter mapping is still legitimate to a large extent in systems where the magnetic moments collectively exhibit small deviations from the collinear case, e.g ferromagnets at low temperatures. Though, as the temperature increases, closing in on the transition temperature, the less and less applicable the mapping becomes, and more clever methods should instead come into use. A temperature dependent Heisenberg exchange coupling was suggested by another research group in 2012 by D. Böttcher and co-workers[41] in which they proposed a systematic way to link electronic structure calculations with Monte Carlo simulations to progress the J_{ij} in temperature. Also, the issue of computing the exchange parameter in systems of strong spin-orbit coupling was discussed in 2003 by L. Udvardi *et al.*[42] via a fully relativistic KKR method which included the sometimes necessary relativistic effects to process the spin-orbit contributions.

2.4 Monte Carlo methods

Modern Monte Carlo methods started to crop up in the 1940s as a mean to estimate analytical theories by taking on a stochastic approach to deal with difficult and analytically unsolvable problems. These methods soon thereafter started to be moulded to fit the scheme of statistical physics which sought a way to probe the intricate phase space of a system by means of stochastic sampling. This meant that random numbers were introduced in the calculations in such a way that the whole phase space could be accessed by some finite probability[43]. A number of algorithms with different areas of applicability have been developed to systematically process this approach and the two that are used in this study are the Metropolis algorithm[44] and the Wang-Landau method[45,46]. Here we will discuss these algorithms based on the Hamiltonian described in section 2.3 and the premises of magnetic system simulations.

2.4.1 Metropolis algorithm

The core of the Metropolis algorithm for a rigid spin system is that it is a methodical process to sort and select the most favourable spin configuration that minimizes the energy output of the Hamiltonian. This is done by first assuming a transition probability equilibrium between successively linked configurations, meaning that there are some collective spin state configurations $\boldsymbol{S}_n$ and $\boldsymbol{S}_m$ that are as likely to transition from the n state to the m state as they are to transition the other way around. Following classical statistical mechanics laid out in section 2.1.2 to first determine the probability of finding the system in state n and m respectively and then impose this transition probability equilibrium one finds that it is of the form

$$P_n W_{n\to m} = P_m W_{m\to n} \tag{34}$$

where P_n is the probability that the system is in state n given by Eq.(15) and $W_{n\to m}$ is the to transition probability going from state n to m[43]. This is known as the detailed balance condition and rearranging it with the explicit form of the canonical probability Eq.(15) one obtains the ratios

$$\frac{W_{n\to m}}{W_{m\to n}} = \frac{P_m}{P_n} = e^{-\beta\Delta E} \tag{35}$$

where $\Delta E = E_m - E_n$ is the relative energy difference between these two states. This puts some constraints on the transition probabilities W, but as long as W is chosen such that it satisfies this condition and every state can be accessed with some finite probability then it is a legitimate choice. One of these choices was made in 1953 by Metropolis *et al.*[44] where they proposed the famed form of the transition probability as

$$W_{n\to m} = \begin{cases} e^{-\beta\Delta E} & ,\text{if} \quad \Delta E > 0 \\ 1 & ,\text{otherwise} \end{cases} \tag{36}$$

This tells us that if the energy difference is negative or equal to zero then there should definitely be a transition from state n to m, while if the energy difference is greater than zero then there is still a probability to transition according

to the Boltzmann distribution shown above[4]. Transforming this scheme into an algorithm that finds the system's energy minimum one may infer that the states are linked to each other in such a way that any new state is generated by its predecessor. This means that any new state that is created is compared with the transition condition in Eq.(36) to see whether or not it replaces the current state configuration. If it does, this new state becomes the reference state in the upcoming computations while if it does not replace the current state then it is discarded, and a new iterative cycle may proceed with the old reference state instead. This chain of linked states is called a Markov chain and its evolution is completely determined by the current state in the process and, with a suitably chosen initial state, should narrow down and converge towards the energy minimum of the Hamiltonian after sufficiently many iterations[43].

Unfortunately, this is not always the case. If the energy landscape of the Hamiltonian is rough meaning that there are deep energy wells that are not the true ground state but difficult for the algorithm to breach through, then the output of the program might not reflect the true energy minimum of the system. This pseudo-minimum could also happen if the program stops before the energy minimum could be reached. In other cases when the ground state is or is almost degenerate with several other states then the program may output different state configurations from run to run and this is especially true for finite temperature simulations. The severity of these problems depends heavily on the complexity of the system of interest, but generally a long chain of iterations is performed to minimize the risk of obtaining a pseudo-minimum, while a great number of reruns of the complete process and averaging the output results produce a better estimate of the system's properties.

Here, a summarized pseudo code of the algorithm is presented with the Heisenberg spin system in mind. Notice that this procedure is only evaluated at a given specified temperature T. This means that several iterations of increasing temperature values need to be performed to properly map the thermodynamic properties of the system.

1. Initialize the lattice by defining a spin configuration and calculate its energy.
2. Choose a random lattice site.
3. Randomize the spin orientation of that site, i.e its spherical angle coordinates $\boldsymbol{s}_i(\phi,\theta) \rightarrow \boldsymbol{s}_i(\widetilde{\phi},\widetilde{\theta})$ and calculate the energy difference ΔE between the two spin configurations.
4. Generate a random number $r \in (0,1)$ and if $r < e^{-\beta\Delta E}$ then keep the new configuration as the current reference, otherwise keep the old orientation and go to (5).
5. Go back to step (2) and reiterate until satisfactory convergence.

2.4.2 Wang-Landau method

A different take on Monte Carlo sampling is the Wang-Landau method that, instead of reiterating over the system's state configurations per temperature step as is necessary for the Metropolis algorithm, focuses on obtaining the temperature independent density of states $g(E)$ discussed in section 2.1.2. This means that as long as $g(E)$ can be determined, all other thermodynamic quantities can be extracted from its corresponding partition function defined in Eq.(14) at any given temperature. This intriguing concept reveals a whole new way of approaching statistical physics problems and offer an alternative numerical algorithm to e.g the Metropolis algorithm.

The general idea of the method is based on the fact that a random walk in energy space with sufficiently many steps will eventually cover the whole energy landscape of the system. Exploiting this concept by modifying the visitation probability of each energy state by a factor inversely proportional to the density of states itself will lead to the formation of a sufficiently uniform visitation-per-energy histogram that is by definition density of state dependent. It will be shown that the final form of the histogram can be used to approximate the shape and form of the system's true density of states.

It begins by first defining the probability to visit a specific energy level E as $P_\mu \propto 1/g(E_\mu)$. This probability is then altered each time that energy is visited by increasing the density of state by a modification factor f_0, such that

$$g(E)_{\text{old}} \rightarrow g(E)_{\text{new}} = g(E)_{\text{old}} f_0 \tag{37}$$

where $f_0 > 0$. This means that the probability to visit that energy level decreases every time the random walker passes by, which in turn causes highly degenerate levels to only reach a certain number of visitations before transitions to more exotic energy states become more probable. The probability to transition from energy E_1 to E_2 within the scheme of the Wang-Landau method with the detailed balance condition is then given by

$$W_{E_1 \rightarrow E_2} = min\left[\frac{g(E_1)}{g(E_2)}, 1\right] \tag{38}$$

After sufficiently many iterations the histogram should have systematically reached a point when it has become somewhat flat. At this stage, the resulting $g(E)$ should have converged towards a good estimate of the system's density of states. To improve these results one may reiterate the procedure with a finer modification factor, e.g $f_1 = \sqrt{f_0}$. The histogram of the previous run is then discarded to start the process anew, but the density of states on the other hand is saved. This will improve the resolution of the final density of states as the modification of the transition probability becomes less rough. When a new "flat" histogram, meaning that it does not differ between its lowest to highest point by more than $\sim 30\%$,

has been achieved one can further polish the density of states with even more reiterations of finer modification factors $f_{i+1} = \sqrt{f_i}$ until satisfactory accuracy[45,46].

Here in this study, the exploration of the energy space is performed by reorienting the spin direction of a randomly chosen spin in our lattice matrix. The system's total energy before and after the spin re-orientation are examined according to Eq.(38) which then determine whether this new energy state is accepted in the random walk scheme of the method. If accepted, then that state configuration becomes the current reference state and its corresponding density of states and histogram are modified with the factor $f_0 = e \approx 2.71828....$ If not, a new random spin is chosen, and the procedure continues as described above. When the complete process is complete, the density of states is normalized to reflect the physically accurate energy degeneracy of the system. This is done by noting that the initial ground state of e.g a ferromagnetic system without external field can only have a collective spin up or spin down configuration, i.e a two-fold degeneracy. After normalizing the density of states to reflect this property, it can then be implemented via the scheme laid out in section 2.1.2 to calculate the desired thermodynamic quantities.

A summarized pseudo code of the algorithm is presented here which follows the rigid spin structure of the Heisenberg model. Notice that many of the parameters are chosen by the user, meaning that the accuracy and computation time is determined by e.g the span in histogram "flatness" and the fine-tuned value of the final modification factor.

1. Choose a condition of histogram "flatness", modification factor f_0 and its desired final value f_{final}.
2. Initialize the lattice with a spin configuration and calculate its energy E_1.
3. Set $g(E) = 1$ for every energy state.
4. Choose a random lattice site.
5. Randomize the spin orientation of that site, i.e its spherical angle coordinates $\boldsymbol{s}_i(\phi, \theta) \rightarrow \boldsymbol{s}_i(\widetilde{\phi}, \widetilde{\theta})$ and calculate the energy of the spin configuration E_2.
6. Determine the transition condition $W_{E_1 \rightarrow E_2}$ according to Eq.(38).
7. Generate a random number $r \in (0, 1)$ and if $r < W_{E_1 \rightarrow E_2}$ then keep the new configuration and modify the histogram and the density of states following Eq.(37), otherwise keep the old orientation and go to (4).
8. If the histogram does not meet the criterion of "flatness", then go to (4). If it does, reduce the modification value by e.g $f_{\text{new}} = \sqrt{f_{\text{old}}}$ and go to (9).
9. Discard the current histogram and repeat (4)-(8) until the modification factor has reached its desired value.
5. Normalize the final $g(E)$ with its exact form at the ground state.

3 Method

This chapter presents the methods and procedures used in this project to conduct the simulations and extract the various magnetocaloric quantities. The first of the following two sections describes the procedure to carry out the magnetic simulations, while the second section addresses the numerical processing of the results, e.g the methods of integration and differentiation. The simulation procedure was executed in two main stages, especially regarding the material realistic simulations, of Fe and CoMnSi. First, spin-polarized ground state electronic structure calculations of a predefined crystal lattice were self-consistently computed, leading to proper extraction of the material specific exchange coupling parameters J_{ij}. In the second stage, the coupling parameters were employed together with the minimal spin Hamiltonian of Eq.(29) to conduct the actual Monte Carlo simulations.

The simple cubic reference system was set up with a lattice parameter of one atomic Bohr radius and a nearest neighbour exchange interaction strength of $1.0mRy$. Next nearest and additional neighbouring interactions were not included. A mean-field estimate of the transition temperature, denoted T_C^* in the results, was calculated via[28]

$$T_C^* = \frac{2}{3} S(S+1) z \frac{J_{nn}}{k_B} \tag{39}$$

in which the spin S was set to the typical electron $\frac{1}{2}$-spin while the number of nearest neighbours, z, was set to six for the simple cubic lattice. The transition temperature estimate tuned out as $T_C^* \approx 473K$.

The two methods of entropy extraction, namely the ΔS derived from the heat capacity of Eq.(24) and ΔS computed via the temperature derivative of the magnetization of Eq.(23), were both calculated for all systems simulated by the Metropolis algorithm. In the simulations governed by the Wang-Landau method, only the ΔS of the heat capacity method was implemented as it was deemed sufficient to cross-check the two algorithms in terms of their main differentiating feature, namely the source of energy computation. The calculated internal energies of these two Monte Carlo methods were then used to determine the heat capacity, which in itself, was calculated in two different ways. One derived from the temperature derivative of the internal energy of Eq.(18) while the other from the variance formula of Eq.(19).

All results concerning the isothermal change in entropy were uniformly shifted such that the low-temperature limit tended towards zero. This action, justified by the fourth postulate of thermodynamics, removes any constants of integration and lets the methods be compared on equal terms.

3.1 Computer simulations

The electronic structure calculations were performed via the so-called *SPR-KKR* software package[47] which utilizes a multiple-scattering KKR Green function formalism to compute the spin-polarized ground state structure by implementing the self-consistency scheme of density functional theory (DFT). The necessary input files to run the *SPR-KKR* program were set up via its included graphical user interface, *XBand*. The crystal data used to construct the materials' crystal lattice was gathered from the Inorganic Crystal Structure Database (ICSD)[48]. The self-consistent calculations were performed in fully relativistic mode using a *spdf*-orbital basis set while implementing the *VWN* local spin density exchange-correlation functional[49]. When the ground state was obtained, the resulting local potentials were used to compute the exchange coupling parameters of the low-temperature state via the LKAG formula, a feature also implemented in the *SPR-KKR* software.

The second stage, i.e the Monte Carlo simulations, were performed using the *UppASD* software[50,51] following the outlined Metropolis and the Wang-Landau algorithms. Here, the lattice structure, exchange coupling parameters and magnetic moments were imported from the output of the *SPR-KKR* results and used to set up the system and the necessary terms in the Hamiltonian of Eq.(29). The Metropolis simulations were thermally equilibrated with about $6 \cdot 10^4$ Monte Carlo lattice sweeps and measured using another $5 \cdot 10^4$ Monte Carlo sweeps. A number of simulations, each with a different pair of temperature and magnetic field values, were performed for each material which meant that the thermodynamic quantities of the system could be mapped out. The Wang-Landau simulations underwent ~ 20 reiteration of the histogram refinement process, ending up with a final modification factor of $f_{20} \approx 1.0000009537$ and a $\sim 80\%$ flat histogram, or until the upper limit of $5 \cdot 10^7$ Monte Carlo steps was reached, in which the last successfully computed histogram was used. The density of states and the partition function were calculated when the final iteration was complete. These quantities were later used to compute the thermodynamic properties of the materials. The Wang-Landau simulations were performed with the same set of magnetic field values as the Metropolis algorithm.

Each material was simulated twice, once with a lattice size of $12 \times 12 \times 12$ cells and another time of size $24 \times 24 \times 24$.

3.2 Numerical post-processing methods

The choice of post-processing methods, especially differentiation, may contribute to additional errors in the final result. Numerical differentiation tends to amplify the inherent errors of discrete data while integration smooths out minor irregularities. These two mathematical operations were necessary tools in this study to properly analyze the Monte Carlo results produced by the simulations. Here, the integrals were computed via a two-point trapezoidal rule

$$\int_a^b f(x)dx \approx \sum_{n=1}^{N} \frac{\Delta x_n}{2} \left[f(x_{n-1}) - f(x_n) \right] \tag{40}$$

in which the length of the subintervals, i.e $\Delta x_n = x_n - x_{n-1}$, were in most cases non-uniform across the span of the temperature and magnetic field intervals.

Differentiation on the other hand, was performed using two different approaches. One of the methods computed the derivatives via a combination of a forward and backward difference rule

$$f'(x_n) \approx \frac{1}{\Delta x_f \Delta x_b} \left[\Delta x_b f(x_{n+1}) + \Delta x_f f(x_{n-1}) + (\Delta x_f - \Delta x_b) f(x_n) \right] \tag{41}$$

where $\Delta x_f = x_{n+1} - x_n$ and $\Delta x_b = x_n - x_{n-1}$. The other method analytically differentiated a set of locally fitted polynomials, computed via the least square fit method around each data point produced in the simulation results. The fit themselves were adjusted such that their order would match the roughness and curvature of the functions in a vicinity around the point of differentiation[52].

4 Results

The following section summarizes the magnetocaloric results of the simulated materials and provides an assessment of the entropy extraction methods. The thermodynamic quantities that are related to differentiation, e.g ΔS via the heat capacity method and ΔT, were computed using the analytical derivative method described in section 3.2, as it was seen that it generally produced more accurate results. The first material under scrutiny is the toy model simple cubic system in which all the entropy extraction methods are put to the test and their differences and similarities discussed. The resolution of the Monte Carlo simulations and the numerical processing methods are investigated in the last part of the simple cubic section. The succeeding parts display the results from the first-principle simulated Fe and CoMnSi materials.

4.1 Simple cubic structure

Figure 3 displays how the phase transition temperature of the 12^3 and 24^3 sized systems shifts to greater temperature values as a consequence of increasing the magnetic field strength. The Curie points shown in these graphs correspond to the extremum points of consecutively computed second-degree polynomials, locally fitted around the sharp divergence peak of the magnetic susceptibility produced from the Metropolis simulations. The critical temperatures of the simple cubic system, regardless of the size of the lattice, exhibit a clear linear dependency with respect to incremental field strengths, all in accordance with what was discussed in section 2.1.1. The Curie points of the larger 24^3 lattice system are more closely condensed around the linear trend than the corresponding set of data of the 12^3 lattice, indicating that the cumulating quantities computed via the Metropolis algorithm become less fluctuating and more precise the larger the system becomes.

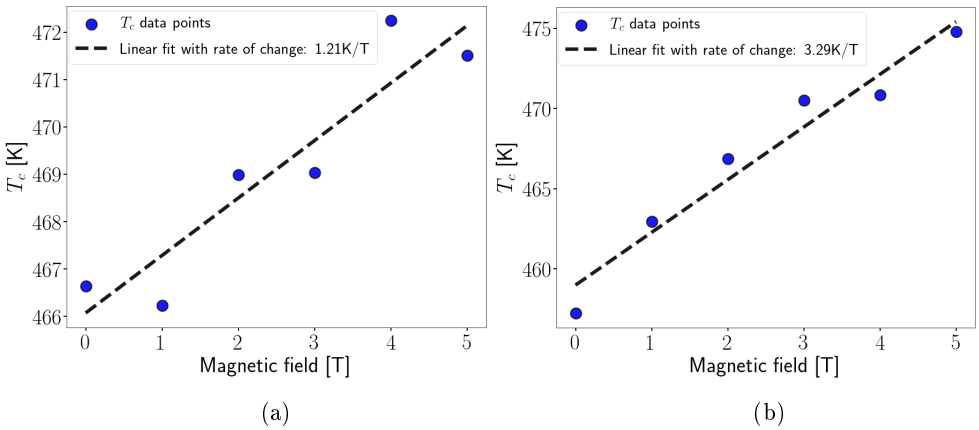

(a) (b)

Figure 3: Graph displaying the change in the Curie temperature for the simple cubic system under the influence of an external magnetic field. The results in Fig. (a) were extracted from a 12^3 lattice system while Fig. (b) from a 24^3 system.

The isothermal change in entropy, and in particular the ΔS affected by the largest considered field variation of $5T$, is displayed in Fig. 4. Here, the two algorithms and the majority of the entropy extraction methods are showing practically the same general traits. A flat and steady low-temperature entropy behaviour which is broken off by an exponentially growing peak around $\sim 460K$, just under the estimated mean field transition temperature. This enhanced large entropy peak around the system's inherent transition point follows the discussed theories of section 2.2, neatly depicting the amplified effects brought forth by driving the magnet in and out of phase. There is one method that deviates significantly from the general behaviour which is the variance heat capacity computed ΔS. The results of this method are shown in relation to the other methods in the embedded graphs in the figures, and will be abbreviated as ΔS_{C^*} from now on. For the 12^3 system, the ΔS_{C^*} shows no sign of a peaked vertex around T_C, though in the 24^3 arrangement, the peak is retrieved but the low-temperature regime is still too irregular to fit with the other methods. Another entropy result that portrays fluctuating features, but to a lesser degree, is the Wang-Landau method computed in the same way as ΔS_{C^*}. This particular method will be referred as ΔS_{WL^*} from now on. It exhibits the familiar peaked trait but at low temperatures, it fluctuates and sometimes deviates considerably from the generally flat and smooth line of the other methods. On the other hand, the ΔS of both the Metropolis and Wang-Landau procedures computed via the heat capacity method, which in turn was determined via the temperature derivative of the internal energy from Eq.(18), show consistent and excellent results regarding the entropy calculations.

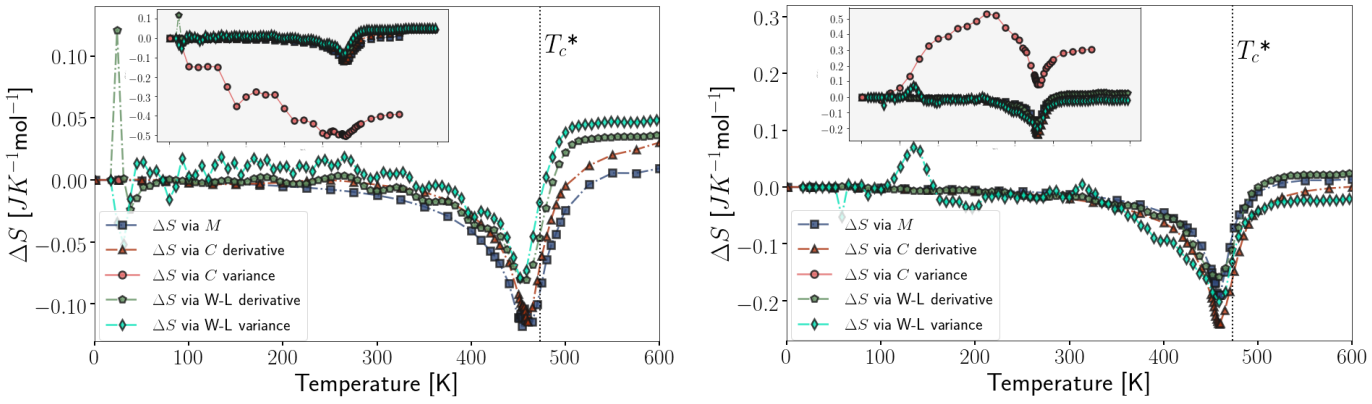

(a) (b)

Figure 4: The isothermal change in entropy under the influence of a field variation of $\Delta H = 5T$ are shown here. Fig. (a) displays ΔS simulated using a 12^3 lattice system while Fig. (b) shows ΔS from a 24^3 system. T_c^* shows the zero field mean-field estimate of the Curie temperature of the simple cubic system. The embedded graphs display a zoomed out version of the original figures that capture the widely deviating behaviour of the heat capacity computed ΔS of Eq.(25) with the heat capacity calculated from the variance formula of Eq.(19).

These two results will here on after be addressed as ΔS_C and ΔS_{WL} respectively. The last method, which will be denoted ΔS_M, corresponds to the change in entropy computed via the temperature derivative of the magnetization from Eq.(23). This method, just as the results from the ΔS_C and ΔS_{WL} approaches, shows promisingly smooth and consistent results. For the smaller system, the 12^3 lattice, the ΔS_M and ΔS_C produce the same absolute peak value value of $\Delta S \approx -0.11\text{JK}^{-1}\text{mol}^{-1}$, while both the Wang-Landau results generate the slightly smaller value of $\sim -0.07\text{JK}^{-1}\text{mol}^{-1}$. For the larger 24^3 system, it is instead the ΔS_C method that stands out. With an entropy variation of $\sim -0.25\text{JK}^{-1}\text{mol}^{-1}$, it trumps the other methods whose values are of the magnitude $\sim -0.18\text{JK}^{-1}\text{mol}^{-1}$.

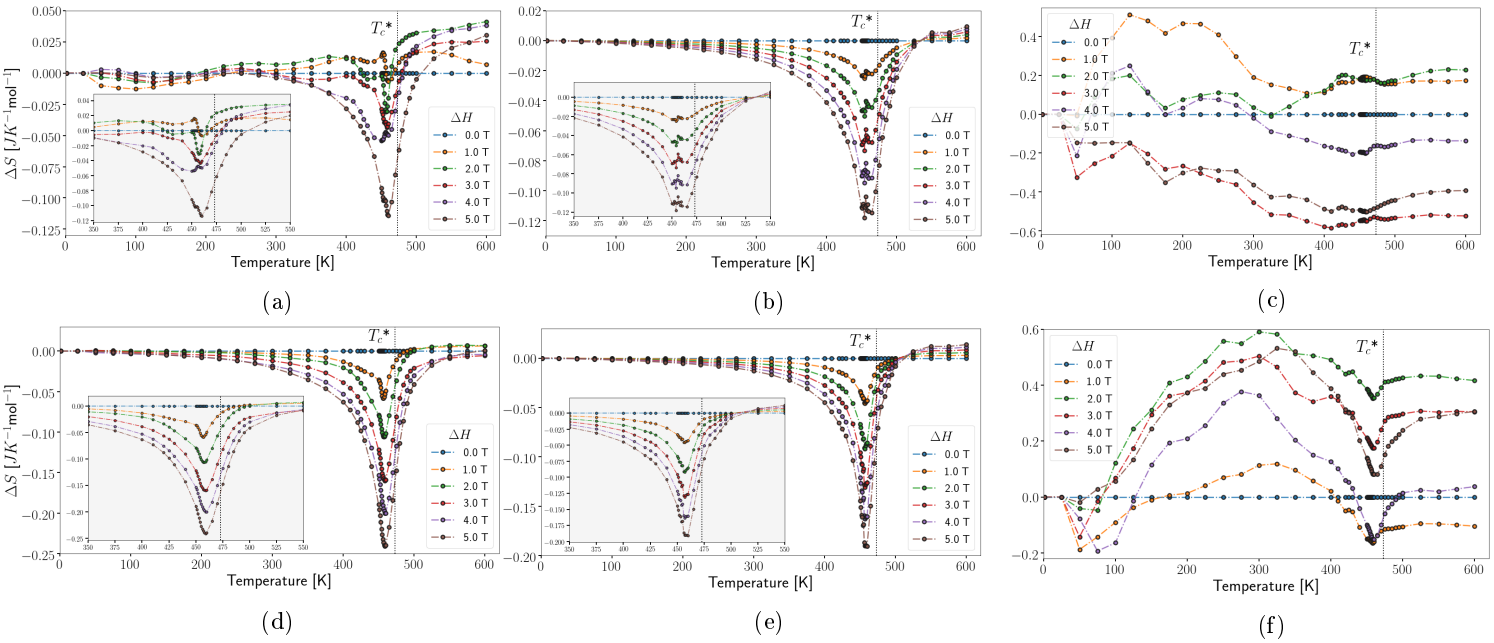

Figure 5: These graphs display the ΔS results, calculated from the Metropolis simulations under varying magnetic field strengths. The results on the top row are computed in a 12^3 lattice system with (a) corresponding to the differentiation heat capacity method ΔS_C, (b) the magnetic order differentiation method ΔS_M and (c) the variance heat capacity method ΔS_{C^*}. Bottom row shows column wise the respective methods but simulated using a 24^3 sized system. The embedded graphs show a zoomed in version of ΔS around the transition peak.

The methods of entropy extraction are not in all cases reliable and universal, even though the results related to the $5T$ field variations display agreeable and promising qualities. The graphs in Fig. 5 show the induced change in entropy under varying field strengths for all the Metropolis computed methods and lattice sizes. Results based on the heat capacity variational method are highly unreliable regardless of lattice size, though as seen previously, ΔS_{C^*} manages to capture the characteristic transition peak in the larger 24^3 system, but is unfortunately too irregular in the low-temperature regime to be evaluated on equal terms with the other methods. The ΔS_C of Fig. 5a only show desired results in the $5T$ field variation. All entropy variations driven by magnetic field values less than this produce irregular and erratic results, but the redeeming familiar qualities are retrieved in the corresponding 24^3 lattice system of

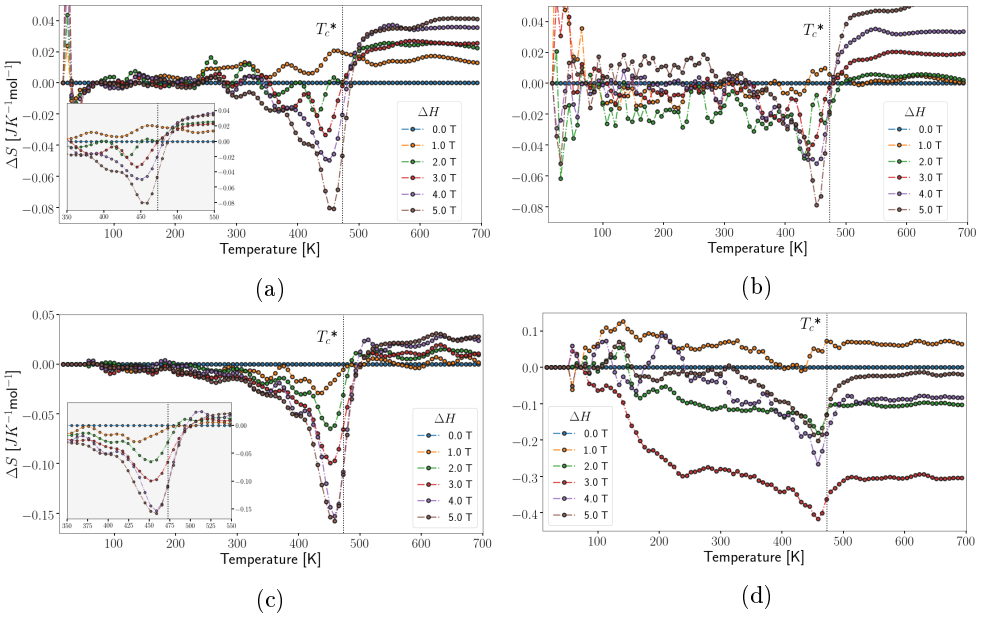

Figure 6: The ΔS of varying magnetic field magnitudes from the Wang-Landau simulations are shown here. The graphs on the top row are computed in a 12^3 system with (a) corresponding to the differentiation heat capacity method ΔS_{WL} and (b) the variance heat capacity method ΔS_{WL^*}. Bottom row shows column wise the respective methods but simulated on the larger 24^3 sized system. The embedded graphs show a zoomed in version of ΔS around the transition peak.

Fig. 5d, where all ΔS, regardless of field variation strength, result in excellent and smooth entropy curves. A particularly reliable method seems to be the ΔS_M approach with the results of both the 12^3 and 24^3 systems demonstrating consistent and accurate entropy variations. Though in the 12^3 of Fig. 5b, the normally distinguishing peak is blurred with minuscule fluctuations, but again, is remedied in the larger lattice system of Fig. 5e.

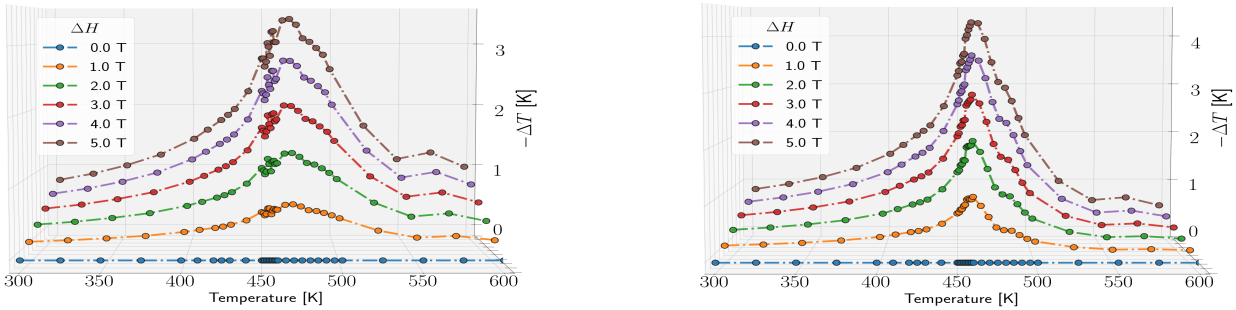

(a) (b)

Figure 7: The adiabatic change in temperature computed via Eq.(28) under the influence of different magnetic field strengths is shown here. Fig. (a) displays ΔT simulated using a 12^3 lattice system with a maximum temperature alteration of $\sim 3.4K$, while Fig. (b) show the temperature change of a 24^3 system with a maximum output of $\sim 4.3K$.

Unlike the smooth entropy changes computed from the systems simulated via the Metropolis algorithm, the Wang-Landau results all show an unfortunate trend regardless of lattice size, which is severe fluctuations throughout the whole temperature interval. For instance, the low magnetic field variations in all graphs of Fig. 6, up to about $2T$, do not reproduce a significantly noticeable peak around T_C, but in its stead are random fluctuations of the same magnitude. The familiar peaked behaviour is brought back under larger field variations, though compared to the results of the Metropolis algorithm, the peak itself is generally broadened and not as sharp. The variance computed results, i.e ΔS_{WL^*}, of both lattice sizes show the same irregularity as the variance computed ΔS_{C^*} of the Metropolis algorithm, but in this case, the peak is somewhat noticeable for both the 12^3 and 24^3 lattice systems.

The final computed thermodynamic quality is the adiabatic change in temperature, ΔT from Eq.(28), which is shown in Fig. 7. The minuscule fluctuations around T_C, seen in Fig. 7a, are caused by the blurred peak behaviour of the temperature derivative of the magnetization, which can also be observed in ΔS_M of Fig. 5b, which are carried along and reproduced in these results. The form of ΔT is much sharper and distinct in Fig. 7b due to the prominent vertex resolution of both the ΔS_M and ΔS_C methods seen in Fig. 5d and Fig. 5e.

Another topic of interest concerning the accuracy of these simulations is the convergence criteria with respect to the number of Monte Carlo steps. Figure 8 display the ΔS_M, ΔS_C and ΔS_{C^*} computed using a 24^3 system with the predefined $5 \cdot 10^4$ Monte Carlo sweeps. The results are compared with simulations performed with a 50% increase and decrease in the number of Monte Carlo steps. The ΔS_M method has converged well in all three simulations while ΔS_C only in the $5 \cdot 10^4$ and $7.5 \cdot 10^4$ ones, leaving the calculations performed with 50% fewer steps dissimilar with the others. The variance method shows again a rough and fluctuating low-temperature behaviour, but the greater $7.5 \cdot 10^4$ Monte Carlo sweep simulation seems to start to take on a similar appearance as the other methods, but it is still not sufficiently smooth in the low-temperature regime.

A comparison between the numerical method of differentiation, computed via Eq.(41), with the analytical derivative of the polynomial fit is shown in Fig. 9. Even though the internal energy of the ΔS_{WL} results were differentiated, the comparison between the numerical and analytical derivatives are omitted here due to the practically identical outcome; a result of the densely sampled temperature points and the general broadened peak of the Wang-Landau method. On the other hand, the ΔS_M and ΔS_C methods display a

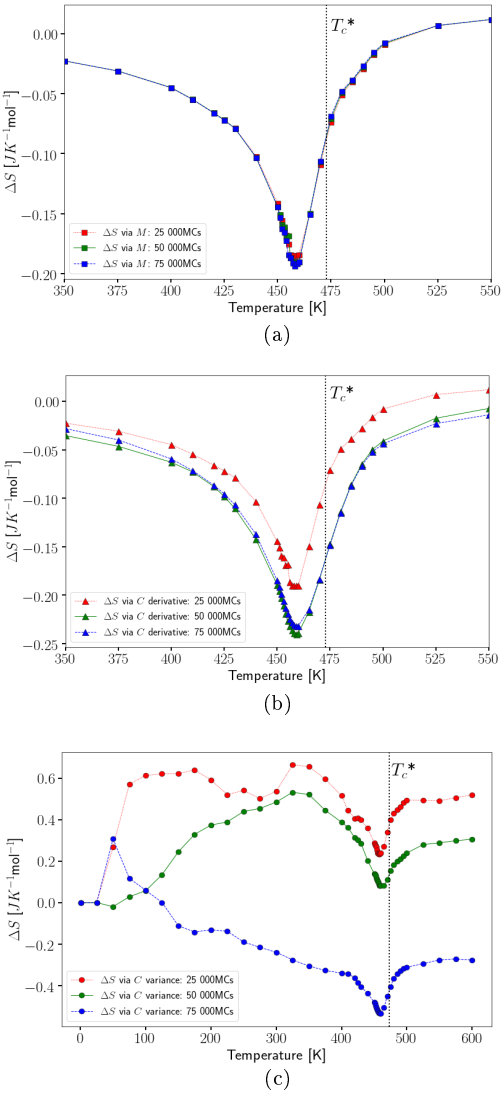

(a) (b) (c)

Figure 8: These figures display the 24^3 lattice ΔS results extracted from simulations of variable number of Monte Carlo sweeps. Figure (a) corresponds to ΔS_M, (b) to ΔS_C and (c) to ΔS_{C^*}.

certain degree of discrepancy, with ΔS_M more severe than ΔS_C. The point around T_C is sufficiently stable in the internal energy derivative of the ΔS_C method to make the peak accurately captured by both differentiation methods, but for the magnetization derivative, the inherent Monte Carlo fluctuations are enhanced in the numerical differentiation. Even the analytical derivative method carries along the fluctuations in the 12^3 system, but the results improve in the larger lattice simulation, reproducing the characteristic divergence peak associated with these types of second order phase transitions.

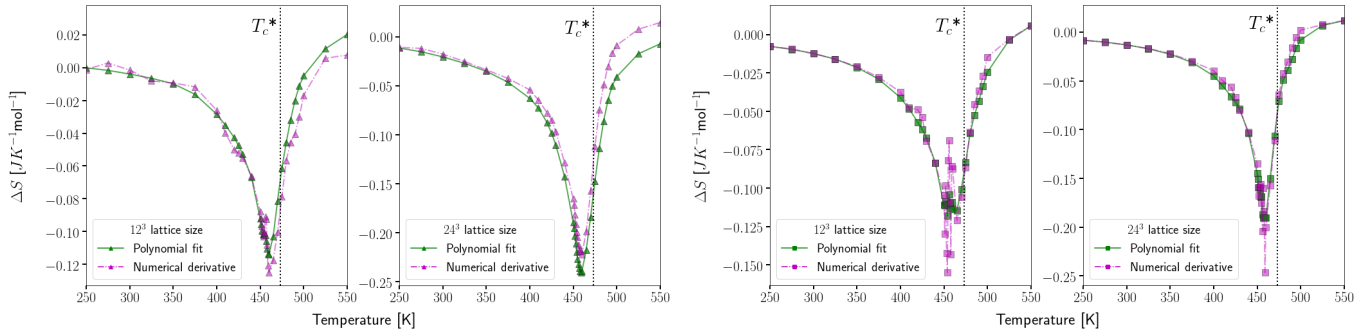

(a) (b)

Figure 9: The numerical post-processing method of differentiation regarding the analytically differentiated polynomial fit and the numerical derivative are compared in these graphs. ΔS_C is displayed in (a) and ΔS_M in (b). Results of both methods were extracted from simulations of a 24^3 sized lattice system.

4.2 Bcc Fe

Figure 10 shows in a similar fashion to the simple cubic results, the varying transition temperature under the influence of external magnetic fields. In this case, the 12^3 system portrays a far more non-linear behaviour than that of the corresponding simple cubic system of Fig. 3, but the transition points of the 24^3 Fe system are in contrast more concisely described by the linear trend. The innate transition temperature of the simulations are underestimated by about $100K$ in comparison with the experimental value of $T_C^E = 1044K$[53].

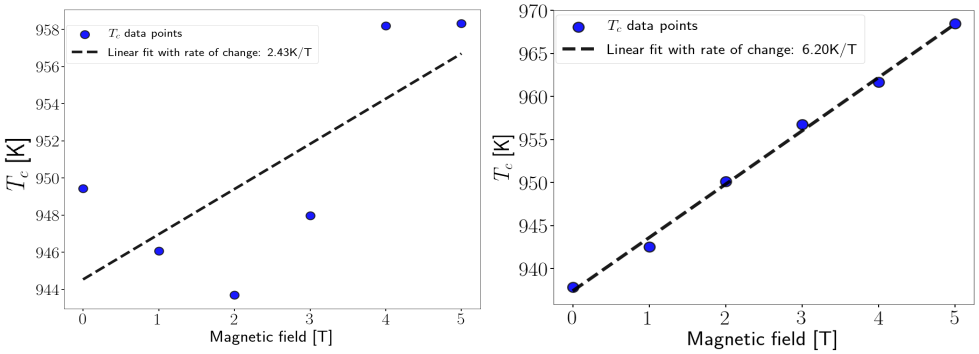

(a) (b)

Figure 10: These graphs display the change in the Curie temperature for the bcc Fe system under the influence of varying external magnetic fields. The results in Fig. (*a*) were extracted from a 12^3 lattice system while Fig. (*b*)shows the Curie points of a 24^3 sized system.

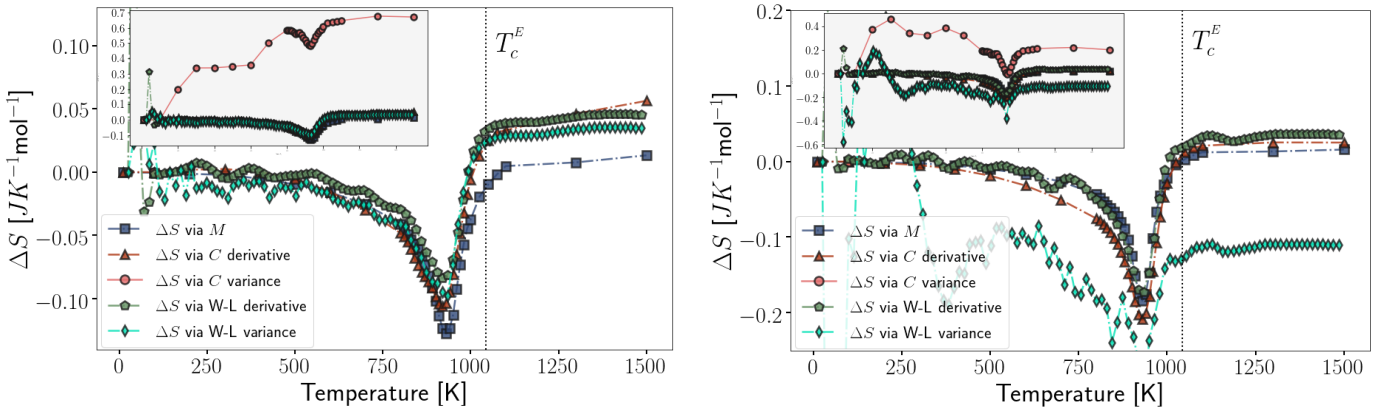

(a) (b)

Figure 11: The isothermal change in entropy of Fe under the influence of a $5T$ magnetic field is shown here. Fig. (*a*) displays ΔS simulated in a 12^3 lattice system and Fig. (*b*) shows ΔS coming from a 24^3 system. $T_C^E = 1044K$ corresponds to the experimentally determined zero field Curie temperature[53].

The results concerning the isothermal change in entropy under a total field variation of $5T$ are displayed in Fig. 11 with the 12^3 system's results on the left and the corresponding 24^3 sized configuration on the right. The characteristic second-order transition peak is seen here centred around $\sim 950K$ and is showing great similarities in shape and form with the one of the simple cubic system. As previously determined, the methods relying on the variance computed heat capacity, in particular ΔS_{C^*}, show no sign of improvement in these material realistic simulations. In the 24^3 sized system, the variance dependent Wang-Landau results show a clear and severe increase in inherent fluctuations, almost reaching the discrepancy of the ΔS_{C^*} method. Surprisingly enough, the same rough behaviour is not found in the smaller 12^3 system, which is the opposite of what was seen in the simple cubic results. The more reliable ΔS_C, ΔS_{WL} and ΔS_M methods produce consistent and similar results, but the ΔS_{WL} method still portrays the minuscule Monte Carlo fluctuations of the Wang-Landau algorithm.

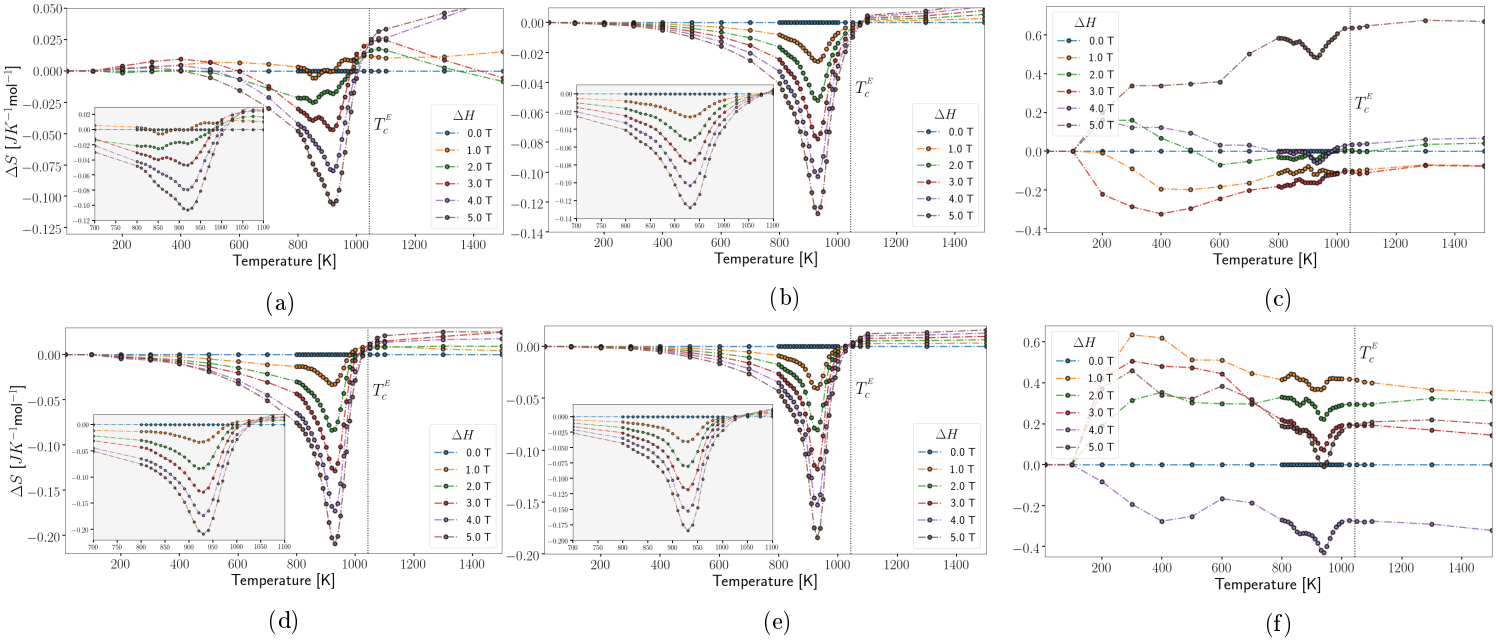

Figure 12: These graphs display the ΔS results of Fe under varying magnetic field strengths, all generated via the Metropolis algorithm. ΔS of the top row were extracted from a 12^3 lattice system with (a) corresponding to the ΔS_C method, (b) the ΔS_M method and (c) the ΔS_{C^*} method. Bottom row displays column wise the respective methods but simulated on the larger 24^3 sized system.

The largest change in entropy in the 12^3 system with a value of $\sim -0.13\text{JK}^{-1}\text{mol}^{-1}$ is produced by the ΔS_M method, however, in the 24^3 system, it is the ΔS_C method that generates the greatest entropy variation with a value of $\sim -0.2\text{JK}^{-1}\text{mol}^{-1}$.

The change in the Fe entropy driven by a number of different external magnetic field values, simulated via the Metropolis algorithm, is shown in Fig. 12. The ΔS_C method of the 12^3 system exhibit some irregularities around T_C, but to a degree far less severe than the results of the corresponding simple cubic case of Fig. 5a. Similar improvements are seen in the ΔS_M method which now shows a more consistent and reliable entropy extraction than in the simple cubic results, where the previously observed fluctuations around the peak have here ceased. The results produced from

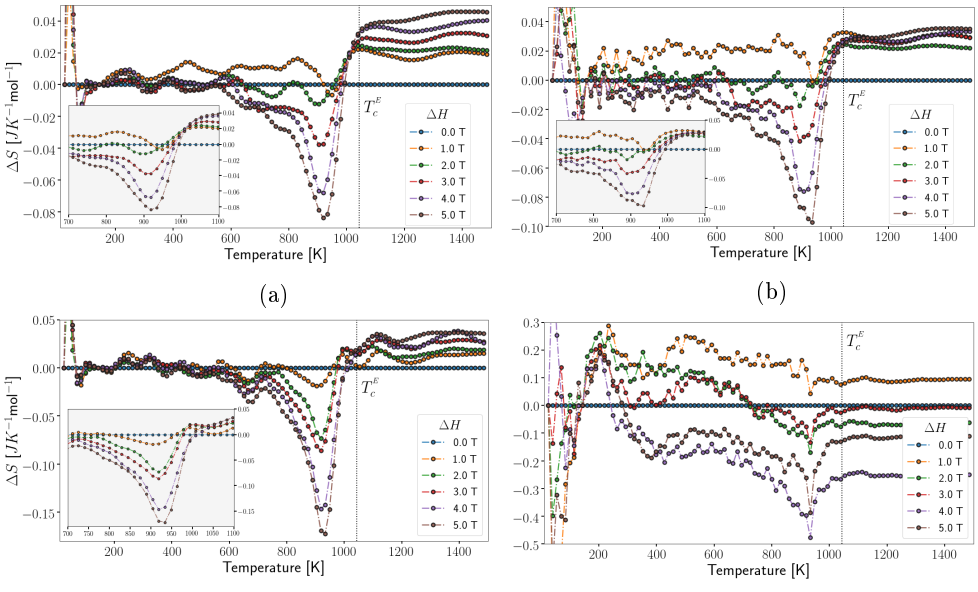

Figure 13: The ΔS of Fe under varying magnetic field strengths from the Wang-Landau simulations are shown here. The graphs on the top row are computed in a 12^3 system with (a) corresponding to the differentiation heat capacity method ΔS_{WL} and (b) the variance heat capacity method ΔS_{WL^*}. Bottom row shows column wise the respective methods but simulated on larger 24^3 sized system.

the Wang-Landau method in the low magnetic field regime $\lesssim 2T$, seen in Fig. 13, still exhibit fluctuations that are of the same amplitude as the entropy output itself, but the peaked behaviour is again retrieved for larger values of ΔH.

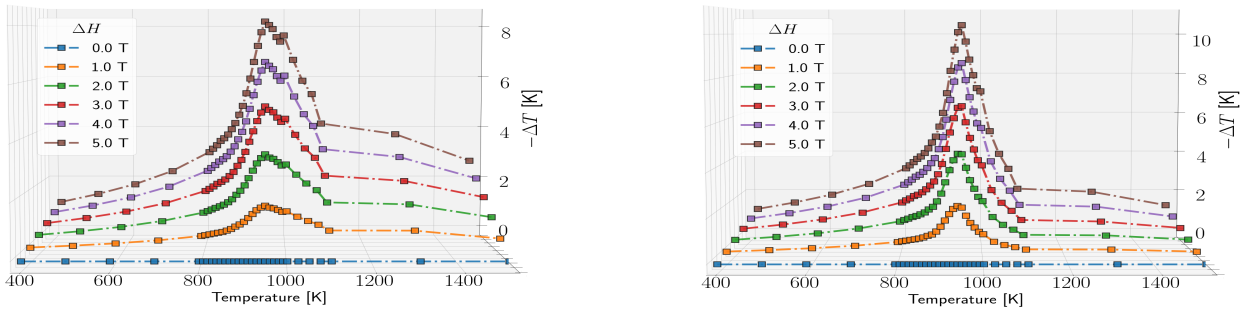

(a) (b)

Figure 14: The adiabatic change in temperature of Fe computed via Eq.(28), using the differentiated heat capacity method, under the influence of different magnetic field strengths are shown here. Fig. (a) display ΔT simulated using a 12^3 lattice system with a maximum temperature alteration of $\sim 8.1K$ while Fig. (b) shows the temperature change of a 24^3 system with a maximum output of $\sim 10.2K$.

The adiabatic change in temperature of the bcc Fe magnet is displayed in Fig. 14. ΔT related to both of the simulated lattice sizes display the signature transition peak but the vertices of the larger system are comparably narrower and steeper in character than those of the 12^3 system. The maximum relative temperature variation goes from $\Delta T \approx 8.1K$ in the 12^3 lattice configuration to $\sim 10.2K$, generated by the larger lattice structure.

4.3 CoMnSi

This last section presents the magnetocaloric qualities of the CoMnSi compound. Simulations of the 24^3 lattice system via the Wang-Landau method were omitted due to too extensive memory usage and lengthy computation times. All other methods are reviewed in a similar fashion as previous results.

The linear shift in the Curie temperature is displayed in Fig. 15. Both of the lattice systems exhibit a clear linear dependency, with the 12^3 configuration having the smallest deviation from the fit

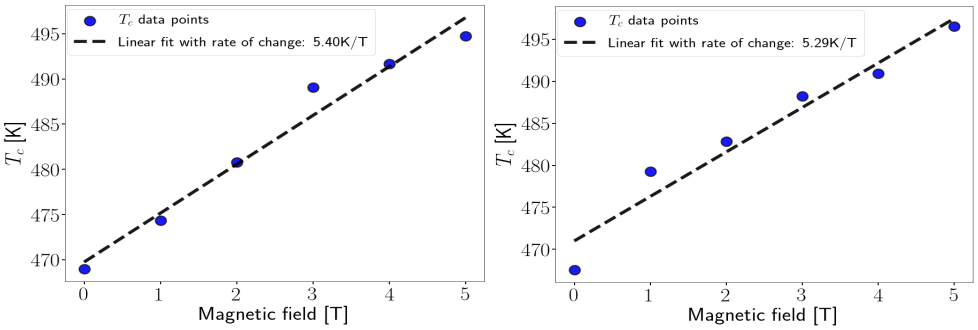

(a) (b)

Figure 15: Graph displaying the change in the Curie temperature for the CoMnSi material driven by variable external magnetic field strengths. The results in Fig. (a) were extracted from a 12^3 lattice system while Fig. (b) shows the Curie points of a 24^3 system.

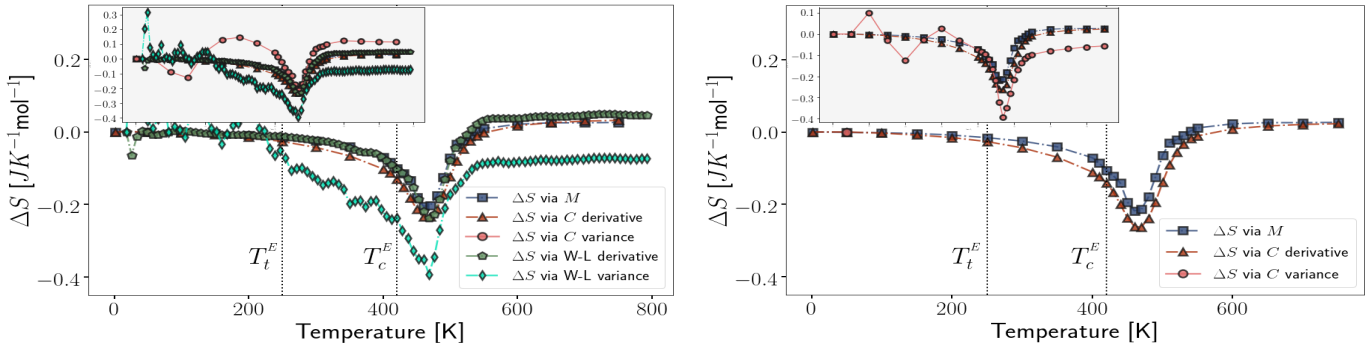

(a) (b)

Figure 16: The isothermal change in entropy of the CoMnSi compound under the influence of a field variation of $\Delta H = 5T$ is shown here. Fig. (a) displays ΔS simulated in a 12^3 lattice system while Fig. (b) shows ΔS coming from a 24^3 system. $T_C^E = 420K$ corresponds to the experimentally determined zero-field Curie temperature, while $T_t^E = 250K$ represents the point of the metamagnetic first order phase transition, converting from an antiferromagnetic to a ferromagnetic state[23].

of all examined materials. Another feature that stands apart compared to the other materials is the matching rate of increase in the transition temperature for the 12^3 and 24^3 lattice systems, indicating that the simulations of the CoMnSi material have converged well in both cases. This quality is found throughout all of the CoMnSi results, where e.g the ΔS method of the two lattice sizes produce almost identical amplitudes and shapes.

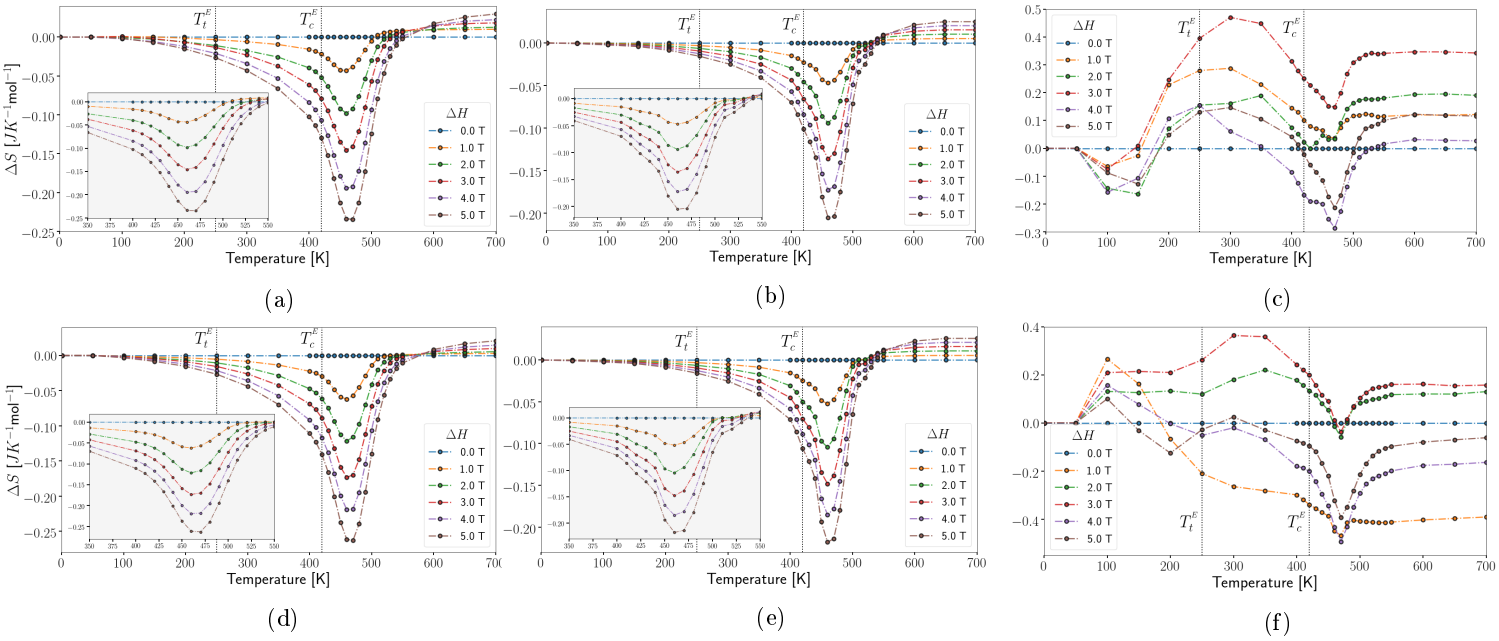

Figure 17: ΔS of CoMnSi calculated from the Metropolis simulations under varying magnetic field strengths are displayed here above. The top row represent the 12^3 lattice system with (a) corresponding to the ΔS_C method, (b) the ΔS_M method and (c) the ΔS_{C^*} method. The bottom row show column wise the respective methods but simulated using a 24^3 sized system.

The change in entropy of the CoMnSi compound, driven by a $5T$ field, is shown in Fig. 16. The T_t^E label in the graphs indicates the position of the experimentally verified metamagnetic first-order magnetic transition, from an antiferromagnetic configuration to a ferromagnetic one, occurring at $\sim 250K$, while T_C^E points out the familiar experimental Curie temperature taking place at $\sim 420K$[23]. As previously established, all ΔS methods, not counting the ΔS_{C^*} and ΔS_{WL^*} procedures, compute the change in entropy in a precise and reliable fashion, with a peaked value of $\sim -0.24\text{JK}^{-1}\text{mol}^{-1}$ produced in the 12^3 lattice system and $\sim -0.27\text{JK}^{-1}\text{mol}^{-1}$ in the 24^3 configuration around $\sim 470K$.

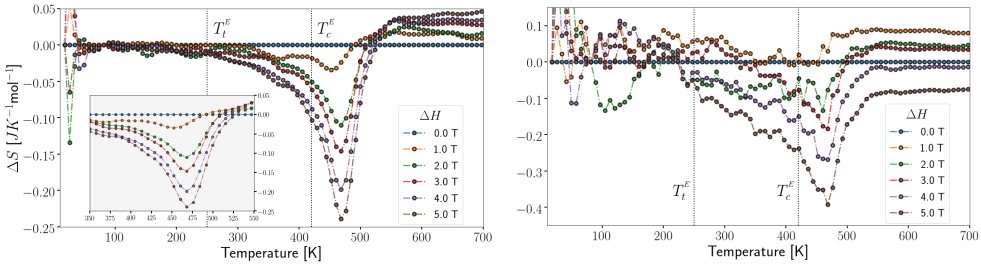

Figure 18: The ΔS_{WL} and ΔS_{WL^*} methods of varying magnetic field strengths of the 12^3 system are shown here on the left and right respectively.

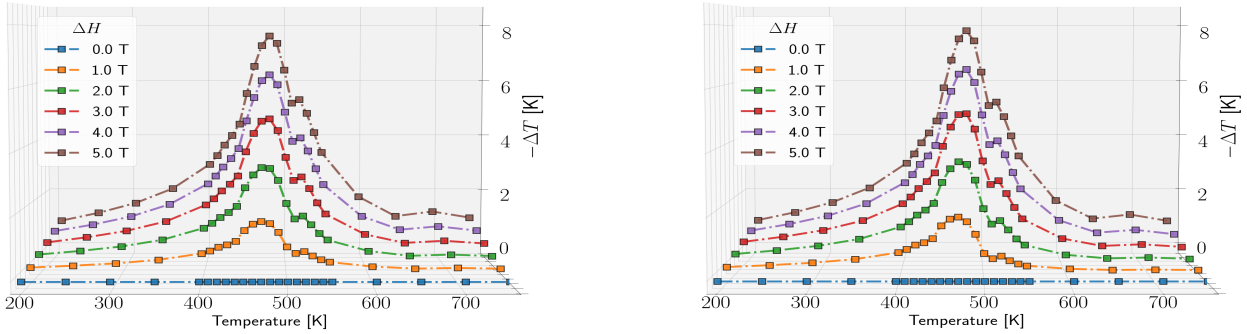

Figure 19: The adiabatic change in temperature of CoMnSi is shown here. Fig. (a) displays ΔT simulated using a 12^3 lattice system and Fig. (b) the 24^3 structure. Both lattice sizes produce a maximum temperature change of $\sim 7.9K$.

The results concerning the adiabatic change in entropy of various field alterations are displayed in Fig. 17 and Fig. 18. The transition peak resolution is greatly improved in these results over those of the Fe and the simple cubic systems as there are no observed Monte Carlo fluctuations around the material's simulated T_C for any of the ΔS_C or ΔS_M methods. ΔS_{WL} still exhibits a great deal of these previously seen defective traits, though compared to the counterpart of the other materials, the peak of the $\Delta H = 2T$ is here quite distinguishable and portray a physically sound general form.

The adiabatic change in temperature of the CoMnSi material is displayed in Fig. 19. Interestingly, the ΔT related to the two lattice systems exhibit practically identical general shapes and forms, with both of them almost reaching a maximum temperature alteration of $8K$.

System and algorithm	Size	Computation time per simulation $[s]$	Number of simulations	Total computation time$[s]$
Simple cubic (Metropolis)	12^3	~ 20	276	5 520
	24^3	~ 60	276	16 560
Simple cubic (Wang-Landau)	12^3	$\sim 11\ 000$	6	66 000
	24^3	$\sim 69\ 000$	6	414 000
Bcc Fe (Metropolis)	12^3	~ 60	276	16 560
	24^3	~ 180	276	49 680
Bcc Fe (Wang-Landau)	12^3	$\sim 10\ 000$	6	60 000
	24^3	$\sim 88\ 000$	6	528 000
CoMnSi (Metropolis)	12^3	~ 500	174	87 000
	24^3	$\sim 5\ 000$	174	870 000
Bcc Fe (Wang-Landau)	12^3	$\sim 92\ 000$	6	552 000
	24^3	-	-	-

Table 2: Computation time estimates of the performed Monte Carlo simulations are displayed here†. The extracted computation times should be regarded as figurative and approximate numbers, solely emphasizing the differences in efficiency of the algorithms.

The last topic that is brought up in this study discusses the efficiency regarding the simulation time of the Metropolis algorithm and the Wang-Landau method. Approximate computation times per Monte Carlo simulation are taken from each considered material and lattice size to appropriately represent the simulation conditions of its category. These estimates, with the total number of considered magnetic field and temperature values, produce a cumulative simulation time which approximately indicates the time scale of the simulations without the use of parallelization, all shown in table 2. The displayed results are by no means fixed values, due to the fact that the convergence criteria of the Monte Carlo methods may differ from simulation to simulation, but also because of varying computation loads that may cause the processing power to drop, and thus also affect the length of the simulations.

5 Discussion

The results concerning the isothermal change in entropy produced by the ΔS_C and ΔS_M methods exhibit very similar and sound general behaviours and the minute discrepancies between them mainly boil down to details of simulation and the discontinuous nature of the phase transitions. This reassuring outcome preserves the theoretical integrity of these two approaches, even though they are originating from different theoretical backgrounds; ΔS_M from thermodynamics and ΔS_C from statistical mechanics. The agreeing nature of these methods can be partially explained by the thermodynamic attributes of the individual terms of the effective spin Hamiltonian. The Heisenberg model establishes the magnetic structure of the material, constituting the source of the exchange governed magnetic ordering, while the Zeeman term provides the system with external stimuli. This means that from a thermodynamical point of view, the Heisenberg model can be regarded as representing the internal energy of the system whereas the Zeeman term corresponds to the work acted upon it. Indeed, by computing the expectation value of the Hamiltonian and taking the exact differential of $\langle \mathcal{H} \rangle$, omitting the field fixed dH contribution, one obtains an expression notably reminiscent of the differential form of the internal energy of Eq.(1). This implies that the statistical mechanics approach, which encompasses all involved interactions within the Hamiltonian notion, also harbours the necessary work terms of a thermodynamic description, leading to the implicit equivalence of the two frameworks, which justifies the identical outcome of these two procedures.

The main deviating features of these two methods are then not caused by some intrinsic theoretical discrepancy, but instead seem to be related to various finite size effects; inconsistencies and errors brought forth due to the limiting finite size of the system when simulated. An example of the misbehaviours associated with these effects can be seen in the

† The simulations were performed on supercomputers at NSC (National Supercomputer Centre) at Linköping, provided by SNIC (Swedish National Infrastructure for computing).

results of the typically linear increase of the Curie temperature. In these results, the smaller 12^3 systems tend to exhibit larger deviations from the fitted linear slope whilst the larger 24^3 systems show good agreement with the linearity of the trend. Another distinguishing finite size problem that is observed for the simple cubic and Fe systems is the enhanced ΔS magnitude of the transition peak of the 24^3 system compared to the smaller 12^3 configuration, sometimes differing up to 100% from one another. This makes it difficult to accurately identify a point in which the system itself starts to properly describe and mimic the bulk properties of the material. In these cases, it might be necessary to implement sophisticated scaling techniques to extract the bulk systems' true thermodynamic properties. This is however not seen in the CoMnSi results, where the ΔS and ΔT of both of the two lattice systems show good agreements with one another, indicating that the simulations might already be representing the bulk of the material. Last side effect of the systems' finite size which will be discussed is directly affecting the precision of the ΔS_C and ΔS_M methods around the transition peak. Here, the Monte Carlo fluctuations occasionally become too severe to produce a reliable reading on the entropy, which is the case for ΔS_C in Fig. 5a, while at other times, such as for ΔS_M in Fig. 5b and ΔS_{WL} in Fig. 6a, the fluctuations are manageable but still too irregular to adequately capture the physics of the phenomena. It seems that in the more material realistic systems the severity of these erroneous effects in the 12^3 lattice systems are reduced, which in turn makes the general shape and form of ΔS more consistent with its reliable 24^3 sized counterpart. For the Fe material, it is mainly the ΔS_C method that still portrays some inconsistencies while the ΔS_M show no sign of fluctuations around T_C. This indicates, at least for the Metropolis algorithm, that an increase in the system size and the inclusion of exchange interactions beyond the nearest neighbour coupling stabilizes the Monte Carlo fluctuations by refining the discrete configuration space and energy landscape of the system. The improved discretization of the energy states produces more closely packed energy levels which in turn makes the energy function of the Hamiltonian smoother, resulting in a more well-defined energy minimum. It is then unlikely that the innate Monte Carlo fluctuations spread too far from this point, making the readings on the energy and magnetization more accurate and dependable. That is why the material realistic magnets, especially the CoMnSi compound and the larger lattice systems, lack the erratic behaviours seen in the simple cubic and smaller 12^3 lattice systems.

Both of the ΔS_C and ΔS_M methods have uniformly proven themselves to be reliable methods of entropy extraction, but on the other side of the spectrum, the methods based on the irregular variance computed heat capacity, namely the ΔS_{C*} and ΔS_{WL^*} methods, are remarkably inadequate in describing the magnetocaloric properties of materials. The severity of the involved fluctuations render the results derived from these procedures highly impractical, and even though the transition peak seems to be satisfactorily described by the ΔS_{C^*} procedure in the larger 24^3 system, the inherent Monte Carlo fluctuations at low temperatures are too unpredictable to deem any of these procedures viable.

The results obtained from the Wang-Landau simulations are generally less attractive than those produced by the Metropolis algorithm due to a couple of reasons. The computed ΔS_{WL} do produce readings on the relative entropy values comparable to the ΔS_C and ΔS_M methods, but its overall shape is unfortunately considerably more irregular as a result of substantial Monte Carlo fluctuations. Another interesting but undesirable feature, seen in the simple cubic and Fe results, is that the transition peak of ΔS_{WL} do not grow in linear proportion to the applied field, a detail that is captured by its Metropolis counterpart, as seen in Fig. 6 and Fig. 13. This particular deficiency does not seem to be a side effect of the finite size of the system, as the results obtained from the larger 24^3 systems also portray the same defective behaviours. The CoMnSi results on the other hand are much better. They exhibit the desired linear growth in ΔS_{WL} with respect to external field seen Fig. 18, but that only holds for field variations of 2T or larger. For all considered materials, the peak of the computed ΔS_{WL} caused by small field variations, $\Delta H \lessapprox 2T$, are in most cases rarely noticeable in the myriad of erratic Monte Carlo fluctuations, and only changes in entropies driven by large fields retrieve the familiar peaked behaviour. Last matter about this procedure to discuss is related to the lengthy computation times of the simulations. Even though the Wang-Landau method requires fewer simulations to adequately map out the thermodynamics of the systems, the exceedingly long computation time per simulation, sometimes up to over 1000 times that of its Metropolis counterpart, render the Wang-Landau algorithm computationally too demanding. Combining these reasons together one may conclude that the Wang-Landau procedure is, unfortunately, an inadequate and ineffective method when studying various magnetocaloric qualities of this type.

The observed over and underestimation of the Curie points might be caused by illegitimate use of the extracted exchange interactions. In all of these simulations, the exchange couplings were taken to be temperature independent and operative at thermally induced non-collinear configurations. In other words, the coupling itself was said to be constant throughout the temperature interval of the simulations and uniquely described by the materials' ground state structures. But it was shown in section 2.3 that it is not possible to completely map a non-collinear magnetic state onto the Heisenberg model alone, making the used approximation less and less valid the closer the simulations get to the paramagnetic transition. For future sake, assuming that the Heisenberg coupling is instead temperature dependent would be an improved approximation that might correct the simulated estimates, despite the fact that it neglects the discussed difficult unique mapping scheme.

Out of the three considered materials, it is only the CoMnSi compound that has been previously studied with respect to its magnetocaloric qualities, as shown in table 1, making it the only material that can be used to compare and benchmark the magnetocaloric results of this study with experiments. The magnitude of the computed ΔS in this study seems to capture the isothermal behaviour of the material, as the change in entropy is remarkably close to its experimental

counterpart, differing with only $\sim 0.07 \mathrm{JK}^{-1}\mathrm{mol}^{-1}$ in value. This makes the *ab inito* approach taken here highly attractive and might very well prove to be a useful method to study magnetocaloric materials at room temperature conditions. The adiabatic change in temperature on the other hand is greatly overestimated in these results, but this comes as no surprise due to two reasons. One is because of the known discrepancies between the direct and indirect estimation of ΔT, where in this case the experimental value was obtained via direct probing, which explains the comparably low-temperature value. The other reason, and the one that makes these two results in fact incompatible with each other, is that the phase transition that was studied in the experiments occurred at the metamagnetic antiferromagnetic to ferromagnetic transition point $T_t^E = 250K$, not at the Curie point $T_C \approx 470K$ which is studied here. This directly points out a substantial flaw in these results which is the absence of an entropy and temperature peak that should have occurred around the material's inherent T_t^E point, expressing the enhanced magnetocaloric properties related to the corresponding first order phase transition. As a consequence of this fact, another flaw that can be observed with this particular simulation is that this approach has determined a ferromagnetic ground state structure and not the experimentally verified antiferromagnetic configuration. This causes the simulations to be unable to properly reproduce the metamagnetic transformation, making the ΔS and ΔT results produced in this study mere estimates of the material's less interesting second order phase transition. This leads us to conclude that the agreeing ΔS results are just coincidental, but the similarity in absolute magnitude still hints that the used procedure might be onto something, making it a potentially accurate method in the study of magnetocaloric materials.

Why the procedure did not capture the metamagnetic transition of the CoMnSi compound might be explained by its troublesome structural transformation at the T_t^E temperature, an effect often simultaneously occurring in conjunction with magnetic first-order phase transitions. It has been seen that the unit cell structure of CoMnSi changes and shrinks across the phases[54], which is not taken into account in these simulations. Unfortunately, structural transitions have proven themselves to be particularly difficult to treat, and accurately describing the phenomena in a self-consistent numerical scheme is no easy feat. This leads us to the shortcomings of the prescribed simulation method. Many of the magnetocaloric qualities of the materials listed in table 1 are partially assisted by structural transitions which amp up the thermodynamic properties of the magnetic first order transitions. This is a characteristic trait of the Heusler alloys, which make them not suited for this type of simulation study. The rare-earth magnets like gadolinium and the lanthanum-based alloys on the other hand do not exhibit this sort of behaviour and could very well be implemented in the used numerical scheme. But these heavier elements come with their own drawbacks, one of which is the matter of the highly localized f-orbitals that cause the rare-earth elements to behave differently than those materials composed of only *spd*-states. The problem emerges in the electronic structure calculations due to correlation effects, meaning that the localized f electrons interact with the itinerant conduction electrons in such a way that an independent electron picture, often associated with the local density approximation (LDA), is no longer a legitimate point of view. The electron states should instead be regarded as connected, or so-called correlated, to one another which complicate the usual electronic structure calculations[55]. Accurately describing the phenomena is in itself an active field of research, and approximate solutions have been developed, such as the Hubbard corrected LDA-U model[56,57], that takes the effect into account, enabling precise calculations of the electronic structure of the rare-earth elements. This implementation has already been adopted in the *SPR-KKR* scheme, making these types of simulations possible.

5.1 Conclusion and outlook

In this study, simulations have been performed with three types of materials, a toy-model simple cubic system, material realistic bcc Fe and CoMnSi compound via two Monte Carlo methods, the Metropolis algorithm and the Wang-Landau method. The ultimate goal was to determine the most suitable method of entropy extraction that would accurately and precisely reflect the magnetocaloric properties of simulated magnetic materials.

Many of the obtained thermodynamic results are in good agreement with theoretical and experimental intuition, while other aspects of these simulations, such as the over and underestimation of the transition points or not being able to capture the first order transitions, leave room for improvements. The computed isothermal changes in entropy on the other hand, have shown that the methods based on differentiation, namely the ΔS_C and ΔS_M methods, produce accurate and reliable results, while those relying on a variance computed heat capacity, i.e ΔS_{C^*} and ΔS_{WL^*}, are inappropriate. The consistency and credibility of the ΔS_C and ΔS_M methods are not to be taken for granted, as finite size effects may affect the complete shape and form of the entropy functions or blur the transition peak with uncertain fluctuations. But generally, the ΔS_M method is the one that produces the most trustworthy results. The magnetocaloric quantities computed via the Wang-Landau algorithm are unfortunately not suitable for scientific investigations due to persistent inherent Monte Carlo fluctuations and lengthy simulation times.

As a concluding remark, even though the simulations failed to identify the point and nature of the experimentally determined ambient phase transition of the CoMnSi compound, the optimistically close entropy values suggest that simulations of this sorts might be worthwhile doing. Further research on the topic by including the rare-earth magnets into the simulation scheme may one day lead the way to an *ab initio* approach in determining novel materials that exhibit substantial magnetocaloric qualities.

References

[1] J C Tolédano and P Tolédano. *The Landau Theory of Phase Transitions*. WORLD SCIENTIFIC, 1987.

[2] X. Moya, S. Kar-Narayan, and N. D. Mathur. Caloric materials near ferroic phase transitions. *Nature Materials*, 13:439 EP –, Apr 2014. Review Article.

[3] M. Balli, S. Jandl, P. Fournier, and A. Kedous-Lebouc. Advanced materials for magnetic cooling: Fundamentals and practical aspects. *Applied Physics Reviews*, 4(2):021305, 2017.

[4] M.E.J. Newman & G.T. Barkema. *Monte Carlo Methods in Statistical Physics*. Oxford Uinversity Press, 1999.

[5] Herbert B Callen. *Thermodynamics and an introduction to thermostatistics; 2nd ed.* Wiley, New York, NY, 1985.

[6] H. Eugene Stanley. *Introduction to phase transitions and critical phenomena, by H. Eugene Stanley*. Clarendon Press Oxford, 1971.

[7] Michael E. McHenry and David E. Laughlin. *Theory of Magnetic Phase Transitions*, pages 1–5. American Cancer Society, 2012.

[8] David P. Landau. *Theory of Magnetic Phase Transitions*. American Cancer Society, 2007.

[9] Pierre Weiss and Auguste Piccard. Le phénomène magnétocalorique. *J. Phys. Theor. Appl.*, 7(1):103–109, 1917.

[10] P. Debye. Einige bemerkungen zur magnetisierung bei tiefer temperatur. *Annalen der Physik*, 386(25):1154–1160, 1926.

[11] W. F. Giauque. A thermodynamic treatment of certain magnetic effects. a proposed method of producing temperatures considerably below 1^o absolute. *Journal of the American Chemical Society*, 49(8):1864–1870, 1927.

[12] W. F. Giauque and D. P. MacDougall. Attainment of temperatures below 1^o absolute by demagnetization of $gd_2(SO_4)_8h_2O$. *Phys. Rev.*, 43:768–768, May 1933.

[13] G. V. Brown and S. S. Papell. Regeneration tests of a room temperature magnetic refrigerator and heat pump. 2014.

[14] Zdeněk Janů and František Soukup. Continuous reading squid magnetometer and its applications. *Review of Scientific Instruments*, 88(6):065104, 2017.

[15] Abd-Elghany Mohamed and Klapötke Thomas M. *psr*, volume 3, chapter A review on differential scanning calorimetry technique and its importance in the field of energetic materials. 2019 2018. 4.

[16] V. Franco, J.S. Blázquez, J.J. Ipus, J.Y. Law, L.M. Moreno-Ramírez, and A. Conde. Magnetocaloric effect: From materials research to refrigeration devices. *Progress in Materials Science*, 93:112 – 232, 2018.

[17] Julia Lyubina. Magnetocaloric materials for energy efficient cooling. *Journal of Physics D: Applied Physics*, 50(5):053002, jan 2017.

[18] S. Fujieda, A. Fujita, and K. Fukamichi. Large magnetocaloric effects in NaZn13-type la(FexSi1-x)13compounds and their hydrides composed of icosahedral clusters. *Science and Technology of Advanced Materials*, 4(4):339–346, jan 2003.

[19] O. Tegus, E. Brück, K. H. J. Buschow, and F. R. de Boer. Transition-metal-based magnetic refrigerants for room-temperature applications. *Nature*, 415(6868):150–152, 2002.

[20] S. Yu. Dan'kov, A. M. Tishin, V. K. Pecharsky, and K. A. Gschneidner. Magnetic phase transitions and the magnetothermal properties of gadolinium. *Phys. Rev. B*, 57:3478–3490, Feb 1998.

[21] A. Fujita, S. Fujieda, Y. Hasegawa, and K. Fukamichi. Itinerant-electron metamagnetic transition and large magnetocaloric effects in $La(fe_xsi_{1-x})_{13}$ compounds and their hydrides. *Phys. Rev. B*, 67:104416, Mar 2003.

[22] Nguyen H. Dung, Zhi Qiang Ou, Luana Caron, Lian Zhang, Dinh T. Cam Thanh, Gilles A. de Wijs, Rob A. de Groot, K. H. Jürgen Buschow, and Ekkes Brück. Mixed magnetism for refrigeration and energy conversion. *Advanced Energy Materials*, 1(6):1215–1219.

[23] K. G. Sandeman, R. Daou, S. Özcan, J. H. Durrell, N. D. Mathur, and D. J. Fray. Negative magnetocaloric effect from highly sensitive metamagnetism in $comnsi_{1-x}ge_x$. *Phys. Rev. B*, 74:224436, Dec 2006.

[24] Feng-xia Hu, Bao-gen Shen, Ji-rong Sun, and Guang-heng Wu. Large magnetic entropy change in a heusler alloy $ni_{52.6}mn_{23.1}ga_{24.3}$ single crystal. *Phys. Rev. B*, 64:132412, Sep 2001.

[25] M. Pasquale, C. P. Sasso, L. H. Lewis, L. Giudici, T. Lograsso, and D. Schlagel. Magnetostructural transition and magnetocaloric effect in $ni_{55}mn_{20}ga_{25}$ single crystals. *Phys. Rev. B*, 72:094435, Sep 2005.

[26] Jian Liu, Tino Gottschall, Konstantin P. Skokov, James D. Moore, and Oliver Gutfleisch. Giant magnetocaloric effect driven by structural transitions. *Nature Materials*, 11:620 EP –, May 2012. Article.

[27] Thorsten Krenke, Eyüp Duman, Mehmet Acet, Eberhard F. Wassermann, Xavier Moya, Lluis Mañosa, and Antoni Planes. Inverse magnetocaloric effect in ferromagnetic ni-mn-sn alloys. *Nature Materials*, 4(6):450–454, 2005.

[28] W. Nolting and A. Ramakanth. *Quantum theory of magnetism*. Springer, New York; Heidelberg, 2009.

[29] M. A. Ruderman and C. Kittel. Indirect exchange coupling of nuclear magnetic moments by conduction electrons. *Phys. Rev.*, 96:99–102, Oct 1954.

[30] Tadao Kasuya. A Theory of Metallic Ferro- and Antiferromagnetism on Zener's Model. *Progress of Theoretical Physics*, 16(1):45–57, 07 1956.

[31] Kei Yosida. Magnetic properties of cu-mn alloys. *Phys. Rev.*, 106:893–898, Jun 1957.

[32] P. Bruno. Theory of interlayer magnetic coupling. *Phys. Rev. B*, 52:411–439, Jul 1995.

[33] A.I. Liechtenstein, M.I. Katsnelson, V.P. Antropov, and V.A. Gubanov. Local spin density functional approach to the theory of exchange interactions in ferromagnetic metals and alloys. *Journal of Magnetism and Magnetic Materials*, 67(1):65 – 74, 1987.

[34] W. Kohn and N. Rostoker. Solution of the schrödinger equation in periodic lattices with an application to metallic lithium. *Phys. Rev.*, 94:1111–1120, Jun 1954.

[35] T. Huhne and H. Ebert. Symmetry properties of the scattering path operator for arbitrary translationally invariant systems. *Phys. Rev. B*, 65:205125, May 2002.

[36] E.N. Economou. *Green's Functions in Quantum Physics*. Springer Series in Solid-State Sciences. Springer, 2006.

[37] Antonios Gonis, William H. Butler, and SpringerLink (Online service). *Multiple Scattering in Solids*. Springer New York, New York, NY, 2000.

[38] A Enders, R Skomski, and J Honolka. Magnetic surface nanostructures. *Journal of Physics: Condensed Matter*, 22(43):433001, oct 2010.

[39] A. Szilva, D. Thonig, P. F. Bessarab, Y. O. Kvashnin, D. C. M. Rodrigues, R. Cardias, M. Pereiro, L. Nordström, A. Bergman, A. B. Klautau, and O. Eriksson. Theory of noncollinear interactions beyond heisenberg exchange: Applications to bcc fe. *Phys. Rev. B*, 96:144413, Oct 2017.

[40] A. Szilva, M. Costa, A. Bergman, L. Szunyogh, L. Nordström, and O. Eriksson. Interatomic exchange interactions for finite-temperature magnetism and nonequilibrium spin dynamics. *Phys. Rev. Lett.*, 111:127204, Sep 2013.

[41] D. Böttcher, A. Ernst, and J. Henk. Temperature-dependent heisenberg exchange coupling constants from linking electronic-structure calculations and monte carlo simulations. *Journal of Magnetism and Magnetic Materials*, 324(4):610 – 615, 2012.

[42] L. Udvardi, L. Szunyogh, K. Palotás, and P. Weinberger. First-principles relativistic study of spin waves in thin magnetic films. *Phys. Rev. B*, 68:104436, Sep 2003.

[43] David P. Landau and Kurt Binder. *A Guide to Monte Carlo Simulations in Statistical Physics*. Cambridge University Press, 4 edition, 2014.

[44] Nicholas Metropolis, Arianna W. Rosenbluth, Marshall N. Rosenbluth, Augusta H. Teller, and Edward Teller. Equation of state calculations by fast computing machines. *The Journal of Chemical Physics*, 21(6):1087–1092, 1953.

[45] Fugao Wang and D. P. Landau. Efficient, multiple-range random walk algorithm to calculate the density of states. *Phys. Rev. Lett.*, 86:2050–2053, Mar 2001.

[46] Fugao Wang and D. P. Landau. Determining the density of states for classical statistical models: A random walk algorithm to produce a flat histogram. *Phys. Rev. E*, 64:056101, Oct 2001.

[47] H Ebert, D Ködderitzsch, and J Minár. Calculating condensed matter properties using the KKR-green's function method, recent developments and applications. *Reports on Progress in Physics*, 74(9):096501, aug 2011.

[48] G Bergerhoff and ID Brown. Crystallographic databases/allen fh et al.(hrsg.). chester, international union of crystallography. 1987.

[49] S. H. Vosko, L. Wilk, and M. Nusair. Accurate spin-dependent electron liquid correlation energies for local spin density calculations: a critical analysis. *Canadian Journal of Physics*, 58(8):1200–1211, 1980.

[50] Olle Eriksson, Anders Bergman, Lars Bergqvist, and Johan Hellsvik. *Atomistic Spin Dynamics: Foundations and Applications*. Oxford University Press, Oxford, 2017.

[51] B Skubic, J Hellsvik, L Nordström, and O Eriksson. A method for atomistic spin dynamics simulations: implementation and examples. *Journal of Physics: Condensed Matter*, 20(31):315203, 2008.

[52] Steven E. Koonin and Dawn Meredith. *Computational physics, FORTRAN version*. Westview Press, Boulder, Co., 1990.

[53] N.W. Ashcroft and N.D. Mermin. *Solid State Physics*. Saunders College, Philadelphia, 1976.

[54] S. Niziol, H. Bińczycka, A. Szytula, J. Todorović, R. Fruchart, J. P. Senateur, and D. Fruchart. Structure magnétique des mncosi. *physica status solidi (a)*, 45(2):591–597, 1978.

[55] Richard M. Martin. *Electronic Structure: Basic Theory and Practical Methods*. Cambridge University Press, 2004.

[56] Vladimir I Anisimov, F Aryasetiawan, and A I Lichtenstein. First-principles calculations of the electronic structure and spectra of strongly correlated systems: the LDA+u method. *Journal of Physics: Condensed Matter*, 9(4):767–808, jan 1997.

[57] Vladimir I. Anisimov, Jan Zaanen, and Ole K. Andersen. Band theory and mott insulators: Hubbard u instead of stoner i. *Phys. Rev. B*, 44:943–954, Jul 1991.